Epilepsy-related CDKL5 deficiency slows synaptic vesicle endocytosis in central nerve terminals

Christiana Kontaxi[a,b,c], Elizabeth C. Davenport[a,b,c], Peter C. Kind[a,b,c], Michael A. Cousin[a,b,c,d*]

[a]Centre for Discovery Brain Sciences, Hugh Robson Building, George Square, University of Edinburgh, Edinburgh EH8 9XD, Scotland, United Kingdom

[b]Muir Maxwell Epilepsy Centre, Hugh Robson Building, George Square, University of Edinburgh, Edinburgh EH8 9XD, Scotland, United Kingdom

[c]Simons Initiative for the Developing Brain, Hugh Robson Building, George Square, University of Edinburgh, Edinburgh EH8 9XD, Scotland, United Kingdom

[d]Lead contact

[*]Correspondence: m.cousin@ed.ac.uk

Summary

Cyclin-dependent kinase-like 5 (CDKL5) deficiency disorder (CDD) is a severe early-onset epileptic encephalopathy resulting mainly from *de novo* mutations in the X-linked *CDKL5* gene. To determine whether loss of presynaptic CDKL5 function contributes to CDD, we examined synaptic vesicle (SV) recycling in primary hippocampal neurons generated from a *Cdkl5* knockout rat model. Using a genetically-encoded reporter, we revealed that CDKL5 is selectively required for efficient SV endocytosis. We showed that CDKL5 kinase activity is both necessary and sufficient for optimal SV endocytosis, since kinase-inactive mutations failed to correct endocytosis in *Cdkl5* knockout neurons, whereas the isolated CDKL5 kinase domain fully restored SV endocytosis kinetics. Finally, we demonstrated that CDKL5-mediated phosphorylation of amphiphysin 1, a putative presynaptic target, is not required for CDKL5-dependent control of SV endocytosis. Overall, our findings reveal a key presynaptic role for CDKL5 kinase activity and enhance our insight into how its dysfunction may culminate in CDD.

Keywords: CDKL5 deficiency, CDKL5 deficiency disorder, kinase, epileptic encephalopathy, synaptic vesicle endocytosis, amphiphysin 1, neurodevelopmental disorders, rat, presynapse, vesicle

Introduction

The majority of neuronal communication occurs at synapses, at which the presynapse contains an abundant number of synaptic vesicles (SVs) loaded with neurotransmitters that are generally released in response to neuronal activity. Following SV fusion, synchronized mechanisms of SV regeneration from the presynaptic plasma membrane guarantee the availability of readily releasable SVs upon repetitive firing and, hence, the fidelity of neurotransmission (Cousin, 2017; Soykan et al., 2016). Neurodevelopmental disorders affect more than 3 % of children worldwide and involve the disturbance of programmed brain development leading to cognitive, social and motor deficits with epileptic seizures being a frequently observed comorbidity (Parenti et al., 2020; Thapar et al., 2017). Mutations in several genes encoding for SV proteins have been identified as causal in the human condition (Baker et al., 2018; Dhindsa et al., 2015; Fassio et al., 2018; Salpietro et al., 2019; Serajee and Huq, 2015). In addition, multiple animal models that exhibit SV trafficking deficits display abnormalities reminiscent of neurodevelopmental conditions (Boumil et al., 2010; Di Paolo et al., 2002; Koch et al., 2011). Therefore, presynaptic dysfunction is emerging as a high-risk factor during neural development.

Cyclin-dependent kinase-like 5 (CDKL5) deficiency disorder (CDD) is a neurodevelopmental and epileptic encephalopathy that is primarily caused by *de novo* single-nucleotide mutations in the X-linked *CDKL5* gene (Fehr et al., 2013). CDD patients largely experience early-onset epileptic seizures and severe neurodevelopmental delay, in addition to a broad spectrum of other clinical manifestations. The human neuron-specific isoform of CDKL5 is a widely expressed serine/threonine kinase, consisting of an N-terminal catalytic domain followed by a long unstructured C-terminal tail (Kilstrup-Nielsen et al., 2012). CDKL5 has been implicated in various neuronal activities, including axon elongation (Nawaz et al., 2016), and synaptogenesis (Zhu et al., 2013). Furthermore, it is proposed to have synaptic roles, with hyperexcitability reported in both excitatory and inhibitory *Cdkl5* conditional knockout (KO) neurons (Tang et al., 2019; Tang et al., 2017). Likewise, upon loss of CDKL5, decreased spontaneous glutamate and GABA efflux is observed in cerebellar synaptosomes (Sivilia et al., 2016). However, a direct role for CDKL5 in SV recycling has not been explored.

Almost all pathogenic mutations in the *CDKL5* gene cluster within the region encoding its kinase domain (Hector et al., 2017), suggesting loss of its enzyme function may be key in CDD. Recently, a limited number of endogenous CDKL5 substrates were identified (Baltussen et al., 2018; Munoz et al., 2018), in addition to a series of *in vitro* targets (Baltussen et al., 2018; Sekiguchi et al., 2013). To date, the only *in vitro* presynaptic target of CDKL5 is amphiphysin 1 (Amph1), on the site serine 293 (S293) within a proline-rich domain (PRD). Amph1 is a cytosolic protein highly enriched in nerve terminals, where it acts as a hub during SV recycling via its multiple interaction domains, including its PRD (Wigge and McMahon, 1998; Wu et al., 2009). Importantly, S293 is a major *in vivo* phosphorylation site on Amph1 and is dephosphorylated during neuronal activity, indicating that it may be of high biological importance (Craft et al., 2008).

68 In the present study, we use a novel *Cdkl5* KO rat model (Simões de Oliveira et al. 2022) to
69 examine SV recycling in CDKL5-deficient hippocampal neurons. Using the genetically-encoded
70 fluorescent reporter synaptophysin-pHluorin (sypHy), we reveal that SV endocytosis is slower
71 upon loss of CDKL5, but SV exocytosis remains unaffected. Following a molecular replacement
72 strategy we demonstrate that the kinase activity of CDKL5 is both necessary and sufficient to
73 correct dysfunction in SV endocytosis. Finally, we determined that the phosphorylation status
74 of Amph1-S293 remains unaltered in CDKL5-null neurons, revealing that CDKL5 exerts its
75 effect on SV endocytosis via a distinct presynaptic substrate. Taken together, our work reveals
76 that CDKL5-mediated phosphorylation is critical for SV endocytosis efficiency, and that CDKL5
77 deficiency is responsible for presynaptic malfunction.

78 ## Results

79 ### Endogenous CDKL5 is sorted into the presynaptic terminal

80 CDKL5 is a ubiquitous neuronal protein kinase (Rusconi et al., 2011; Schroeder et al., 2019)
81 however, its localisation at the nerve terminal has not been extensively addressed. To verify
82 that CDKL5 is present in presynaptic terminals, and therefore in the correct location to
83 influence SV recycling, a classical subcellular fractionation was performed. During this
84 protocol, an adult rat brain was subjected to homogenisation and differential centrifugation
85 to generate distinct subcellular fractions, including a crude synaptosome- (P2, mainly
86 representing the presynapse with attached postsynaptic density) and an SV-enriched (LP2)
87 fraction. Western blotting with a CDKL5-specific antibody (**Figure S1**) revealed that CDKL5 was
88 present in the P2 fraction and enriched in the LP2 fraction, where the SV protein
89 synaptophysin 1 (Syp1) also accumulated (**Figure 1A**). The relative absence of the
90 postsynaptic marker, postsynaptic density 95 (PSD95), suggested that contamination of the
91 LP2 fraction with postsynaptic elements was limited. Therefore, CDKL5 is present at
92 presynaptic terminals and may associate with SVs, consistent with previous studies showing
93 that CDKL5 colocalises with the presynaptic vesicular glutamate transporter 1 (VGLUT1) in
94 mouse neurons (Ricciardi et al., 2012; Wang et al., 2021).

95 To assess whether CDKL5 is targeted exclusively to nerve terminals or displays a more diffuse
96 axonal distribution, we performed coefficient of variance (CV) analysis. Hippocampal neurons
97 were transfected with either CDKL5 fused to the fluorescent protein mCerulean (mCer-
98 CDKL5), Syp1-mCer or the empty mCer vector and were then immunolabelled for the
99 presence of the fluorescent tag (**Figure 1B**). SV proteins, such as Syp1, are anticipated to have
100 a punctate distribution along the axon and therefore a higher CV value. In contrast, lower CV
101 values indicate a homogeneous distribution of a protein along the axon. In agreement, mCer-
102 Syp1 displayed a localised distribution along the axon and a high CV value, in agreement with
103 previous results (Gordon and Cousin, 2013). Quantification of the distribution profile of CDKL5
104 in axonal segments indicated a CV value similar to the empty mCer vector (**Figure 1C**).
105 Therefore, CDKL5 is diffusely distributed along the axon, including presynaptic terminals.

106 **Loss of CDKL5 does not influence the levels of presynaptic proteins or the number of**
107 **presynaptic boutons**

108 We next investigated whether the absence of CDKL5 causes any defects in presynaptic
109 stability since disruption of synapse stability/synaptogenesis may result in altered neuronal
110 development. This was important to address, since dysregulation of protein levels in addition
111 to altered synapse number have been reported in mice lacking CDKL5 (Della Sala et al., 2016;
112 Ren et al., 2019; Schroeder et al., 2019; Tang et al., 2019). First, we examined whether
113 expression of key presynaptic proteins was altered in rat CDKL5 KO neurons via Western
114 blotting. Initially, we confirmed the absence of CDKL5 in lysates of KO neurons (**Figure 2A**).
115 We then analysed a range of presynaptic molecules including proteins important for SV
116 recycling, such as clathrin heavy chain (CHC), dynamin 1 (Dyn1), endophilin A1, and syndapin
117 1; integral SV proteins, such as Syp1, VGLUT1, and the v-type proton ATPase subunit B
118 (ATP6V1B2); and phosphoproteins that have been implicated in the regulation of SV
119 endocytosis, such as the protein kinases glycogen synthase kinase 3 (GSK3) and Akt (Clayton
120 et al., 2010; Ferreira et al., 2021; Smillie and Cousin, 2012). These latter enzymes were of
121 particular interest, since the PI3K/GSK3/Akt pathway has been one of the most perturbed
122 signalling cascades in CDKL5 deficiency model systems (Amendola et al., 2014; Jiang et al.,
123 2019; Wang et al., 2012). This analysis revealed that the absence of CDKL5 did not significantly
124 alter the total protein level of any candidate, or the phosphorylation status (and thus activity)
125 of either GSK3 or Akt when compared to wild-type (WT) controls (**Figure 2A**). Therefore CDKL5
126 KO neurons do not display overt alterations in presynaptic proteins or signalling cascades.

127 Next, we investigated whether the lack of CDKL5 led to a reduced number of presynaptic
128 terminals. To achieve this, WT and CDKL5 KO neurons were double-stained for two distinct
129 presynaptic markers, synaptic vesicle protein 2A (SV2A) and VGLUT1, to assess the number of
130 presynaptic boutons and excitatory presynaptic subtypes, respectively. There were no
131 genotype-specific differences in SV2A- and VGLUT1-positive puncta along neuronal processes
132 (**Figure 2B**). Therefore, there is no effect of the absence of CDKL5 on either the number of
133 total or excitatory presynaptic terminals (**Figure 2C, D**). Overall, this data reveals that the
134 formation and maintenance of nerve terminals in rat primary neuronal cultures is not affected
135 upon CDKL5 deficiency.

136 **Loss of CDKL5 impairs SV regeneration but does not influence SV exocytosis**

137 The presynaptic localisation of CDKL5 suggests that CDKL5 is implicated in SV recycling.
138 Indeed, phenotypes reported in mice lacking CDKL5, such as altered frequency of
139 spontaneous and miniature postsynaptic currents (mPSCs) (Tang et al., 2017; Wang et al.,
140 2021), and aberrant paired-pulse facilitation (Tang et al., 2019), indicate that CDKL5 deficiency
141 results in defects in synaptic transmission that could be due to dysfunctional SV recycling. To
142 determine this, we used the genetically-encoded reporter sypHy, in which a pH-sensitive form
143 of GFP, ecliptic pHluorin (pKa ~7.1), is inserted into an intravesicular loop of Syp1 (Granseth
144 et al., 2006; Miesenbock et al., 1998). The fluorescence of sypHy is dictated by the pH of its
145 immediate environment, with fluorescence being quenched in the acidic SV lumen,
146 unquenched upon stimulus-dependent SV exocytosis and exposure to the cell surface, and

147 re-quenched following endocytosis and SV acidification (**Figure 3A**). To determine the
148 potential contribution of CDKL5 to SV recycling across a range of stimulus intensities, primary
149 hippocampal neurons derived from CDKL5 KO rats or WT littermate controls were transfected
150 with sypHy and stimulated with action potential (AP) trains of either 5 Hz or 10 Hz (both 300
151 APs) or 40 Hz (400 APs) (**Figure 3B, E, H**). To quantify for the extent of activity-dependent SV
152 exocytosis, the amount of sypHy fluorescence during stimulation was measured as a
153 proportion of the total fluorescence within the presynapse revealed by perfusion with NH_4Cl
154 that allows for an estimation of the total recycling SV pool. We found that the extent of SV
155 exocytosis remained unaltered between genotypes across all stimulation frequencies
156 investigated (**Figure 3C, F, I**). To confirm this phenotype, we next measured the rate of sypHy
157 fluorescence increase during prolonged stimulation (10 Hz for 90 s) in the presence of
158 bafilomycin A1. Bafilomycin A1 is a V-type ATPase inhibitor, and therefore removes any
159 potential contribution from SV endocytosis to the sypHy response during the stimulation by
160 blocking SV acidification (Sankaranarayanan and Ryan, 2001). When this experiment was
161 performed, no difference was observed in either the rate of the sypHy fluorescence increase
162 (SV exocytosis rate) or the extent of the sypHy response (SV recycling pool size) between WT
163 and CDKL5 KO neurons (**Figure S2A, B, C**). Therefore, SV exocytosis is not altered upon CDKL5
164 loss.

165 We next focused on SV endocytosis, in which protein kinases perform an important role
166 (Clayton et al., 2010; Tan et al., 2003). As acidification is a rapid process when compared to
167 rate-limiting SV endocytosis (Atluri and Ryan, 2006; Egashira et al., 2015; Granseth et al.,
168 2006), monitoring the sypHy fluorescence decay after stimulation can be used to estimate SV
169 endocytosis kinetics (Sankaranarayanan and Ryan, 2000). To quantify the kinetics of SV
170 retrieval, the sypHy stimulation peak was normalised, and the amount of sypHy remaining to
171 be retrieved 2 minutes after termination of stimulation was measured. This parameter was
172 used for consistency across protocols, since in specific cases the decay kinetics were not
173 mono-exponential (rendering time constant measurements redundant). CDKL5 KO neurons
174 consistently displayed slower SV endocytosis across all frequencies examined when
175 compared to WT, suggesting that CDKL5 is important for optimal SV endocytosis (**Figure 3D,**
176 **G, J**). Interestingly, the requirement for CDKL5 appeared to be more prominent at lower
177 stimulation frequencies.

178 To confirm that this phenotype was due to slowed SV endocytosis and not dysfunctional SV
179 acidification, we determined the kinetics of SV acidification using an acid-pulse protocol
180 (Granseth et al., 2006). In this protocol, an impermeant acid buffer (pH 5.5) is perfused
181 immediately after stimulation to quench all surface sypHy, which exclusively reveals the
182 sypHy signal inside recently retrieved SVs (where the quenching rate can be calculated). In
183 this protocol WT and CDKL5 KO neurons expressing sypHy are perfused with acid buffer both
184 prior to stimulation (to reveal an initial baseline) and immediately after stimulation (10 Hz, 30
185 s, to reveal the quenching rate inside SVs) (**Figure S2D**). No significant difference in the SV
186 acidification rate in neurons lacking CDKL5 compared to WT neurons was apparent (**Figure**
187 **S2E**), confirming that the slowing in the post-stimulus sypHy fluorescence decay in CDKL5 KO
188 neurons was due to impaired SV endocytosis.

189 CDD is a disorder of early life, and a therefore key question to address is whether defects can
190 be rescued by the re-introduction of the gene, or whether the altered circuit activity in its
191 absence renders gene correction redundant. To address this in our system, we determined
192 whether expression of WT CDKL5 in KO neurons could correct SV endocytosis deficits. Both
193 CDKL5 KO and WT littermate controls were co-transfected with sypHy and either mCer-CDKL5
194 or an empty mCer vector and stimulated with either 300 APs at 10 Hz or 400 APs at 40 Hz.
195 Analysis of the post-stimulus sypHy response showed that expression of mCer-CDKL5 fully
196 restored the kinetics of SV endocytosis after 10 Hz stimulation and partially after 40 Hz.
197 Importantly, mCer-CDKL5 overexpression had no impact on SV endocytosis kinetics in WT
198 neurons, indicating that increased levels of the protein kinase had no dominant negative
199 effect (**Figure 4A-D**). Thus, expression of CDKL5 can restore presynaptic defects observed in
200 KO neurons.

201 **CDD-related mutants of CDKL5 fail to rescue SV endocytosis impairment**

202 As stated above, in CDD all identified pathogenic missense mutations are found within the
203 kinase domain suggesting the disorder is due to loss of its enzymatic function (Hector et al.,
204 2017; Munoz et al., 2018). To determine whether the protein kinase activity of CDKL5 is
205 essential for its role in SV endocytosis, we investigated the ability of two mutant forms of full-
206 length CDKL5 to restore function in CDKL5 KO neurons. The CDKL5 mutants were 1) K42R (a
207 catalytically-inactive form of the enzyme that cannot bind ATP (Lin et al., 2005)), and 2) R178P,
208 a mutation reported in CDD patients of both sexes with severe neurological features (Elia et
209 al., 2008; Nemos et al., 2009) (**Figure 5A**). CDKL5 KO neurons were co-transfected with sypHy
210 and either WT CDKL5 or one of the CDKL5 mutants and SV endocytosis kinetics were
211 monitored following stimulation with either 300 APs at 10 Hz or 400 APs at 40 Hz (**Figure 5B,**
212 **D**). WT CDKL5 fully restored SV endocytosis kinetics after both stimulation trains, as observed
213 previously. In contrast, neither of the CDKL5 mutants were able to correct the SV endocytosis
214 defect (**Figure 5C, E**). The absence of rescue was not due to their low expression, since this
215 was equivalent to the exogenously-expressed WT enzyme (**Figure S3**). These data reveal that
216 the protein kinase activity of CDKL5 is essential for optimal SV endocytosis kinetics and also
217 associates CDKL5 pathology with defective SV recycling.

218 **The kinase activity of CDKL5 is necessary and sufficient for optimal SV endocytosis**

219 We have revealed an essential requirement for the enzymatic activity of CDKL5 in SV
220 endocytosis. However a key question to address is whether this activity is both necessary and
221 sufficient to correct SV endocytosis dysfunction in CDKL5 KO neurons. To address this, we
222 examined whether expression of the isolated protein kinase domain was sufficient to correct
223 presynaptic function in CDKL5 KO neurons. To determine this, we generated mCer-tagged
224 deletion mutants of CDKL5 comprising either the kinase domain (ΔC; aa 1-297) or the C-
225 terminal tail (Δkinase; aa 298-960) (**Figure 6A**). Primary cultures of hippocampal CDKL5 KO
226 neurons were co-transfected with sypHy and either full-length CDKL5 or one of the deletion
227 mutants. Double immunostaining of primary cultured hippocampal neurons for GFP and
228 endogenous CDKL5 suggested that Δkinase was expressed to higher levels than WT, whereas

229 ΔC could not be quantified due to the absence of an antibody epitope (**Figure S3**). SV
230 endocytosis kinetics were assessed by monitoring sypHy fluorescence after stimulation with
231 300 APs at 10 Hz or 400 APs at 40 Hz (**Figure 6B, D**). We observed that the isolated kinase
232 domain was sufficient to rescue SV endocytosis kinetics similarly to full-length CDKL5 at both
233 stimulus intensities (**Figure 6C, E**). In contrast, the isolated C-terminus could not, suggesting
234 that this region cannot support SV endocytosis in the absence of the protein kinase domain.
235 Therefore, the ability of the isolated CDKL5 protein kinase domain to correct presynaptic
236 function reveals that it is both necessary and sufficient to rescue SV endocytosis, and that the
237 C-terminal tail is dispensable for this role.

238 **CDKL5-mediated phosphorylation at Amph1-S293 is not required for SV regeneration**

239 Since the kinase activity of CDKL5 is necessary for optimal SV endocytosis, this suggests that
240 there is at least one CDKL5 substrate at the presynapse that mediates this role. The only
241 candidate presynaptic target of CDKL5 that has been identified so far is Amph1, from *in vitro*
242 studies (Katayama et al., 2015; Sekiguchi et al., 2013). To determine whether Amph1 may be
243 a *bona fide* CDKL5 substrate, we first examined the ability of these two proteins to interact
244 with each other, as it would be anticipated for an enzyme to interact with its substrates, even
245 transiently. We demonstrated reciprocal co-immunoprecipitation of Amph1 and CDKL5 from
246 rat brain lysates (**Figure 7A**). This indicates that CDKL5 binds to Amph1 *in vivo*, and hence
247 supports that Amph1 may be a CDKL5 substrate.

248 Previous studies determined Amph1-S293 as the residue phosphorylated by CDKL5 *in vitro*
249 (Katayama et al., 2015; Sekiguchi et al., 2013), which also resides within a CDKL5 consensus
250 motif (Baltussen et al., 2018; Munoz et al., 2018). Furthermore, Amph1-S293 appears to be a
251 plausible CDKL5 target in relation to its potential role in SV endocytosis, since its
252 phosphorylation status regulates the affinity of Amph1 for the presynaptic endocytosis
253 protein endophilin A1 (Murakami et al., 2006; Sekiguchi et al., 2013). To explore CDKL5-
254 mediated phosphorylation of Amph1, we generated a rabbit polyclonal phospho-specific
255 antibody against Amph1-S293 (**Figure S4A**). To validate this antibody, we generated
256 recombinant GST-conjugated constructs of the central region of WT Amph1 that
257 encompassed this site (residues 248-620, GST-Amph1) and two phospho-mutants, a null (GST-
258 S293A) and a mimetic (GST-S293E) and assessed its specificity by Western blotting. This
259 approach revealed that the pAmph1-S293 antibody reacted exclusively with the phospho-
260 mimetic GST-S293E (**Figure S4B**), suggesting that the phospho-antibody is highly specific for
261 phosphorylated Amph1-S293.

262 Amph1 undergoes dephosphorylation coupled to neuronal activity (Bauerfeind et al., 1997;
263 Micheva et al., 1997). Accordingly, Amph1-S293 is one of the phospho-sites that is
264 dephosphorylated following high frequency stimulation (Craft et al., 2008; Murakami et al.,
265 2006). Therefore, we next focused on verifying whether Amph1-S293 was dephosphorylated
266 in an activity-dependent manner. Initially, we treated hippocampal neuronal cultures with 50
267 mM KCl for 2 min to induce neuronal depolarisation. This greatly reduced the signal from the
268 pAmph1-S293 antibody when compared to basal cultures, suggesting that the antibody
269 accurately reports the phosphorylation status of this residue. We next examined whether

270 Amph1-S293 dephosphorylation occurs via calcineurin, since this Ca^{2+}-dependent enzyme
271 dephosphorylates a series of presynaptic proteins during neuronal activity (Bauerfeind et al.,
272 1997; Cousin and Robinson, 2001; Marks and McMahon, 1998; Nichols et al., 1994).
273 Treatment with cyclosporin A, a calcineurin inhibitor, prevented the activity-dependent
274 dephosphorylation at Amph1-S293, confirming that calcineurin performs this role. In
275 contrast, treatment with calyculin A, an inhibitor of protein phosphatases 1 and 2A that are
276 responsible for the main phosphatase activity in presynaptic terminals under basal and
277 depolarising conditions, failed to prevent Amph1-S293 dephosphorylation (**Figure S4C**).
278 Additionally, we examined the impact of electrical field stimulation, during which neurons
279 were stimulated with 300 APs at 10 Hz or 400 APs at 40 Hz in the presence or absence of the
280 antagonists AP5 and CNQX (which prevent postsynaptic activity or recurrent spontaneous
281 activity). We observed that Amph1-S293 was dephosphorylated after stimulation at both
282 frequencies (**Figure S4D**). Furthermore, the phosphorylation profile of Amph1-S293 was
283 similar to that of pDyn1-S774, an established phosphorylation site that undergoes calcineurin-
284 and activity-dependent dephosphorylation (Clayton et al., 2009; Liu et al., 1994; Tan et al.,
285 2003). Overall, these findings suggest that Amph1-S293 undergoes calcineurin-mediated
286 dephosphorylation linked to neuronal activity at the presynapse.

287 To assess whether Amph1-S293 is a CDKL5 substrate, WT and CDKL5 KO neuronal cultures
288 were stimulated with 50 mM KCl and allowed to repolarise for different periods of increased
289 duration to determine whether the absence of CDKL5 impacted on rephosphorylation of this
290 residue (**Figure 7B**). KCl stimulation was employed to ensure complete dephosphorylation of
291 S293, providing the widest possible dynamic range to visualise changes in its
292 rephosphorylation. A phospho-antibody against the established endogenous CDKL5 substrate
293 microtubule-associated protein 1S (MAP1S)-S900 was also used as a positive control
294 (Baltussen et al., 2018; Munoz et al., 2018). In WT neurons, Amph1-S293 was efficiently
295 rephosphorylated within 2.5 minutes after KCl stimulation (**Figure 7C**). In CDKL5 KO neurons
296 there was no significant change in the phosphorylation levels of Amph1-S293 either before,
297 during or after the KCl stimulus when compared to WT controls (**Figure 7C**). In contrast,
298 phosphorylation of MAP1S-S900 was eliminated in CDKL5 KO neurons in all conditions. This
299 supports the conclusion that Amph1-S293 is not directly phosphorylated by CDKL5 *in vivo* and,
300 therefore, this phospho-site does not play a significant role in the slowing of SV endocytosis
301 due to CDKL5 deficiency.

302 **Amph1-S293 is phosphorylated independently of CDKL5 at the presynapse**

303 The unaltered phosphorylation levels of Amph1-S293 in the absence of CDKL5 indicates that
304 another protein kinase is responsible for its phosphorylation *in vivo*. However, it is also
305 possible that a different protein kinase substitutes for CDKL5 activity in CDKL5 KO neurons. A
306 number of early studies showed that there are two protein kinases that phosphorylate
307 Amph1-S293 *in vitro* in addition to CDKL5, including dual-specificity tyrosine phosphorylation-
308 regulated kinase 1A (Dyrk1A) (Murakami et al., 2006) and mitogen-activated protein kinase
309 (MAPK) (Shang et al., 2004), whereas cyclin-dependent kinase 5 (Cdk5) (Floyd et al., 2001;
310 Liang et al., 2007) is also reported as an Amph1 kinase in mature neurons. In an attempt to
311 unmask any potential phosphorylation of Amph1-S293 and to determine whether other

312 protein kinases may substitute for CDKL5 in its absence, we treated WT and CDKL5 KO
313 neurons with a cocktail of protein kinase inhibitors, including epigallocatechin gallate (EGCG),
314 PD98059, and roscovitine to simultaneously eliminate the kinase activity of Dyrk1A, MAPK,
315 and Cdk5, respectively (**Figure 7D**). KCl-induced depolarisation of WT and CDKL5 KO neurons
316 was followed by repolarisation for 10 min (Error! Reference source not found.**Figure 7E**). We
317 revealed that the phosphorylation levels of pAmph1-S293 were not altered between
318 genotypes when normalised to total Amph1, as previously observed (**Figure 7F**). Moreover,
319 the cocktail of kinase inhibitors abolished the rephosphorylation of pAmph1-S293 post-
320 stimulation, indicating that kinases other than CDKL5 phosphorylate this residue in WT
321 neurons and the contribution of CDKL5 to its phosphorylation is minor, if any. Importantly,
322 the unaltered phosphorylation of the endogenous CDKL5 substrate pMAP1S-S900 (Baltussen
323 et al., 2018; Munoz et al., 2018) in the presence of inhibitors excludes the possibility these
324 inhibitors to act on CDKL5. Collectively, these data suggest that at least one presynaptic kinase
325 other than CDKL5 phosphorylates pAmph1-S293 at hippocampal neurons.

326 ## Discussion

327 CDD is emerging as a prominent monogenic neurodevelopmental and epileptic
328 encephalopathy, therefore determining the key biological roles of CDKL5 will be vital in
329 developing targeted therapies. In this work, we reveal the first direct role for CDKL5 at the
330 presynapse, the control of SV regeneration. This requirement was specific to SV regeneration,
331 with no other aspects of the SV life cycle impacted by the absence of the kinase. This defect
332 in CDKL5 KO neurons was stimulus-independent, suggesting CDKL5 performs a fundamental
333 role in the facilitation of this process. Importantly, CDKL5 protein kinase activity was both
334 necessary and sufficient for this role, suggesting that CDKL5-dependent phosphorylation
335 performs a fundamental role in facilitating SV turnover during neuronal activity.

336 A number of postsynaptic defects has been observed in a series of CDKL5 KO model systems,
337 such as increased (Okuda et al., 2017; Yennawar et al., 2019) or decreased (Della Sala et al.,
338 2016) long-term potentiation, altered dendritic morphology/dynamics (Amendola et al.,
339 2014; Della Sala et al., 2016; Tang et al., 2017; Terzic et al., 2021), upregulated NMDA receptor
340 number (Okuda et al., 2017; Tang et al., 2019; Terzic et al., 2021) and a shift in AMPA receptor
341 subunit composition (Yennawar et al., 2019). Furthermore, a number of studies have
342 suggested that loss of CDKL5 impacts synapse numbers in specific brain regions. Alterations
343 in synapse number have been proposed to modulate the frequency of miniature events in
344 systems where CDKL5 is absent (Della Sala et al., 2016; Ricciardi et al., 2012). However, in our
345 primary neuronal culture system, we observe no obvious change in synapse number via
346 staining with the presynaptic marker SV2A. Our study takes advantage of a novel rodent
347 system to model CDD, a CDKL5 KO rat. A full characterisation of the electrophysiological and
348 behavioural phenotypes of the CDKL5 rat model is described here (Simões de Oliveira et al.
349 2022), however similarly to other constitutive CDKL5 KO models, they do not display overt
350 seizure activity. Hippocampal brain slices from this model system do display reduced mEPSC
351 frequency with no apparent decrease in synapse number (Simões de Oliveira et al. 2022),

352 suggesting that this defect may be linked to dysfunctional SV regeneration rather than less
353 available synapses.

354 We revealed that the kinase activity of CDKL5 is necessary and sufficient for its role in SV
355 regeneration. This was achieved via use of structural/patient mutations and expression of
356 isolated domains in molecular replacement studies. The K42R mutant is a *bona fide* kinase
357 dead protein since it fails to bind ATP and phosphorylate targets *in vitro* (Lin et al., 2005). The
358 patient mutation R178P (Elia et al., 2008; Nemos et al., 2009) is also assumed to be kinase
359 dead since a similar patient mutation (R178W) abolished kinase activity *in vitro* (Munoz et al.,
360 2018). However the kinase activity of this specific mutant still has to be directly investigated.
361 The ability of the isolated CDKL5 kinase domain to fully restore presynaptic function was
362 surprising, and suggests that the unstructured C-terminus, which forms the majority of the
363 protein, is dispensable for CDKL5 localisation and/or substrate recognition. Importantly,
364 overexpression of full-length protein did not affect SV regeneration, suggesting increased
365 gene dosage is not deleterious to presynaptic function. These findings have important
366 implications for future gene therapy studies, since insertion of the isolated kinase domain will
367 facilitate packaging inside viral delivery vectors that have limited space. The potential of this
368 strategy to have therapeutic benefits in individuals with CDD is supported by studies where
369 re-expression of the CDKL5 gene in KO mice fully reversed a cohort of cell, circuit and
370 behavioural phenotypes (Terzic et al., 2021). The finding that CDD appears to be a disorder of
371 neuromaintenance and not neurodevelopment (Kind and Bird, 2021), provides support that
372 expression of the CDKL5 kinase domain later in life may restore specific aspects of brain
373 function.

374 We also revealed that S293 on Amph1 is not the CDKL5 substrate that controls SV
375 regeneration. This site was an excellent candidate, since it was situated within a CDKL5
376 consensus sequence, is phosphorylated by the kinase *in vitro* (Katayama et al., 2015; Sekiguchi
377 et al., 2013) and is the dominant *in vivo* site on Amph1 (Craft et al., 2008). Furthermore, this
378 site is dephosphorylated during neuronal activity (Craft et al., 2008; Murakami et al., 2006)
379 and its phosphorylation status controls interactions with the endocytosis protein endophilin
380 (Murakami et al., 2006; Sekiguchi et al., 2013). Finally, deficiency of Amph1 results in
381 occurrence of irreversible seizures in mice (Di Paolo et al., 2002). However, phospho-specific
382 antibodies against S293 revealed no change in its phosphorylation status in CDKL5 KO
383 neurons. A series of *in vitro* studies have identified other candidate proteins kinases that could
384 phosphorylate this site (Floyd et al., 2001; Liang et al., 2007; Murakami et al., 2006; Shang et
385 al., 2004). An inhibitor cocktail containing antagonists of these protein kinases abolished
386 rephosphorylation of Amph1 S293 in both WT and CDKL5 KO neurons, suggesting that these
387 protein kinases do not substitute for CDKL5 in its absence. Given the interplay between CDKL5
388 and Dyrk1A (Oi et al., 2017; Trovo et al., 2020), we also excluded the possibility that CDKL5
389 loss may influence the phosphorylation of Amph1-S293 by Dyrk1A. The identity of the protein
390 kinase that rephosphorylates S293 is still therefore undetermined, however it is clear that its
391 phosphorylation does not mediate CDKL5-dependent effects on SV regeneration. The identity
392 of the presynaptic CDKL5 substrate(s) is currently under investigation.

One interesting observation was that the impact of loss of CDKL5 function on SV regeneration appeared to reduce with increasing stimulus frequencies. Remarkably, CDKL5 is not the only kinase of the CMGC (named after the initials of some member kinases) group that has been reported to behave in a frequency-dependent manner. For example, overexpression of Dyrk1A results in more profound SV endocytosis delay following low rather than high frequencies in hippocampal neurons (Kim et al., 2010). This is an intriguing observation, since defects in SV endocytosis are typically exacerbated with increased stimulus intensities (McAdam et al., 2020; Zhao et al., 2014). Since GABAergic neurons usually fire at higher frequencies (Bartos et al., 2007), this suggests that excitatory neurotransmission may be disproportionately affected by the absence of CDKL5. Recent studies in conditional CDKL5 KO models provide some support to this hypothesis. For example, selective deletion of CDKL5 in inhibitory interneurons increases mEPSC, but not mIPSC frequency (Tang et al., 2019). Furthermore, conditional KO of CDKL5 in mouse excitatory neurons resulted in overt seizure phenotypes (with increased mEPSCs, but not mIPSCs), whereas the equivalent deletion in inhibitory neurons had little effect (Wang et al., 2021). Therefore there appears to be a complex relationship between loss of CDKL5 function when examined at the level of intact brain circuits. Consequently, it may be too soon to predict how defects in presynaptic SV regeneration culminate in both global and specific circuit dysfunction and ultimately seizure activity in individuals with CDD.

In summary, we have identified a key presynaptic role for CDKL5 in neurotransmission and potentially circuit and brain function. It will be critical to determine the molecular target(s) of this kinase within this specialised subcellular region to determine the extent that presynaptic dysfunction underpins this neurodevelopmental and epileptic encephalopathy.

Acknowledgements

This work was supported by grants from the Loulou Foundation, the Simons Foundation (529508), The Wellcome Trust (204954/Z/16/Z) and a College of Medicine and Veterinary Medicine studentship to CK. For the purpose of open access; the author has applied a CC-BY public copyright license to any author accepted manuscript version arising from this submission. We thank Lynsey Dunsmore for help with maintenance of the *Cdkl5* KO LE colony and Dr. Sally Till for her help with the cortices dissection. We also thank Dr Ira Milosevic and Dr Giles Hardingham for useful suggestions in an earlier version of this work.

Author Contributions

Conceptualization, PCK, MAC; Methodology CK, ECD, MAC; Data analysis, CK; Visualisation, CK; Investigation, CK, MAC; Resources, PCK; Writing, CK, MAC; Funding Acquisition, PCK, MAC.

Declaration of Interests

The authors declare no competing interests.

430 **Star Methods**

431 **Key Resources Table**

REAGENT or RESOURCE	SOURCE	IDENTIFIER
Antibodies		
Chicken anti-GFP	Abcam	Cat# ab13970, RRID:AB_300798
Donkey anti-goat IRDye 680RD	LI-COR Biosciences	Cat# 925-68074, RRID:AB_2650427
Donkey anti-goat IRDye 800CW	LI-COR Biosciences	Cat# 925-32214, RRID:AB_2687553
Donkey anti-guinea pig IRDye 680RD	LI-COR Biosciences	Cat# 925-68077, RRID:AB_2814914
Donkey anti-mouse IRDye 680RD	LI-COR Biosciences	Cat# 925-68072, RRID:AB_2814912
Donkey anti-mouse IRDye 800CW	LI-COR Biosciences	Cat# 925-32212, RRID:AB_2716622
Donkey anti-rabbit Alexa Fluor 488	Molecular Probes, Thermo Fisher Scientific	Cat# A-21206, RRID:AB_2535792
Donkey anti-rabbit IRDye 680RD	LI-COR Biosciences	Cat# 925-68073, RRID:AB_2716687
Donkey anti-rabbit IRDye 800CW	LI-COR Biosciences	Cat# 925-32213, RRID:AB_2715510
Donkey anti-sheep Alexa Fluor 568	Molecular Probes, Thermo Fisher Scientific	Cat# A-21099, RRID:AB_2535753
Goat anti-Amph1	Santa Cruz Biotechnology	Cat# sc-8536, RRID:AB_2226798
Goat anti-CHC	Santa Cruz Biotechnology	Cat# sc-6579, RRID:AB_2083170
Goat anti-chicken Alexa Fluor 488	Molecular Probes, Thermo Fisher Scientific	Cat# A-11039, RRID:AB_142924
Goat anti-Dyn1	Santa Cruz Biotechnology	Cat# sc-6402, RRID:AB_639941
Goat anti-EHD	Santa Cruz Biotechnology	Cat# sc-23452, RRID:AB_2097347
Goat anti-guinea pig Alexa Fluor 568	Molecular Probes, Thermo Fisher Scientific	Cat# A-11075, RRID:AB_141954
Goat anti-syndapin 1	Santa Cruz Biotechnology	Cat# sc-10412, RRID:AB_653788
Guinea pig anti-VGLUT1	Synaptic Systems	Cat# 135 304, RRID:AB_887878
Mouse anti-PSD95	BioLegend	Cat# 810401, RRID:AB_2564750
Mouse anti-β-actin-peroxidase	Sigma-Aldrich	Cat# A3854, RRID:AB_262011
Rabbit anti-ATP6V1B2	Abcam	Cat# ab183887
Rabbit anti-CDKL5	Atlas Antibodies	Cat#HPA002847, RRID:AB_1080107
Rabbit anti-pAkt-S473	Cell signalling	Cat# 9018, RRID:AB_2629283
Rabbit anti-pAmph1-S293	MRC Protein Phosphorylation Unit, University of Dundee, UK	N/A
Rabbit anti-pGSK3α/β-S9/S21	Cell signalling	Cat# 9331, RRID:AB_329830
Rabbit anti-pMAP1S (light chain)-S900	Rouse lab, University of Dundee, UK	N/A
Rabbit anti-sheep IRDye800 conjugated	Rockland Immunochemicals	Cat# 613-732-168, RRID:AB_220182
Rabbit anti-SV2A	Abcam	Cat# ab32942, RRID:AB_778192
Rabbit anti-Syp1	Abcam	Cat# ab14692, RRID:AB_301417
Sheep anti-CDKL5 (Human epitope)	Rouse lab, University of Dundee, UK	N/A
Sheep anti-CDKL5 (Mouse epitope)	Rouse lab, University of Dundee, UK	N/A
Sheep anti-pDyn1-S774	AbD Serotec (Bio-rad)	Cat# AHP899, RRID:AB_567392
Chemicals, peptides, and recombinant proteins		
B-27™ Supplement (50X), serum free	Gibco™, ThermoFisher Scientific	Cat# 17504044
Bafilomycin A1	Alfa Aesar	Cat# J61835.MX
Boric Acid	Sigma-Aldrich	Cat# B6768
Bovine serum albumin	Roche Diagnostics GmbH	Cat# 10735078001
Bradford	AppliChem	Cat# A6932
Calyculin A	Abcam	Cat# ab141784
Cyano-7-nitroquinoxaline-2,3-dione	Abcam	Cat# ab120271
Cyclosporin A	Sigma-Aldrich	Cat# 30024
Cytosine arabinofuranoside	Sigma-Aldrich	Cat# C1768
Dimethyl sulfoxide	Sigma-Aldrich	Cat# D8418
Dithiothreitol	Sigma-Aldrich	Cat# D0632
DL-2-Amino-5-phosphonopentanoic acid	Abcam	Cat# ab120044
DMEM-F12	Gibco	Cat# 21331-020
Epigallocatechin gallate	Calbiochem	Cat# 324880-10MG
Foetal Bovine serum	BioSera	Cat# S1810-500
Glutathione Sepharose 4B beads	GE Healthcare	Cat# GE17-0756-01
Instant Blue™ Protein Stain	C.B.S. Scientific	Cat# HG73010
Intercept (PBS) Blocking Buffer	LI-COR Biosciences	Cat# 927-70001
Intercept (TBS) Blocking Buffer	LI-COR Biosciences	Cat# 927-60001
Isopropyl β-D-1-thiogalactopyranoside	Calbiochem	Cat# 420322
Laminin	Sigma-Aldrich	Cat# L2020
L-glutamine	Gibco	Cat# 25030-024
Lipofectamine 2000	ThermoFisher Scientific	Cat# 11668027

Lysozyme	Sigma-Aldrich	Cat# L6876
Neurobasal	Gibco	Cat# 21103-049
Papain	Worthington Biochemical Corporation	Cat# LK003178
PD98059	EMD Millipore Corp.,	Cat# 513000-5MG
Penicillin/Streptomycin	Gibco	Cat# 15140-122
Poly-D-lysine	Sigma-Aldrich	Cat# P7886
Ponceau-S staining	Sigma-Aldrich	Cat# P7170
ProbeQuant G-50 Micro Column	GE Healthcare	Cat# 28903408
Protease inhibitor cocktail	Sigma-Aldrich	Cat# P8849
Protein G Agarose beads	Sigma-Aldrich	Cat# 11719416001
Roscovitine	EMD Millipore Corp.	Cat# 557360-1MG
Experimental Models: organisms/strains		
Mouse: C57Bl/6J	Charles River, UK	N/A
Rat: *Cdkl5* KO LE, Long-Evans	Horizon Discovery, USA	N/A
Rat: Sprague Dawley	Charles River, UK	N/A
Recombinant DNA		
GST-Amph1	This paper	N/A
GST-Amph1 S293A	This paper	N/A
GST-Amph1 S293E	This paper	N/A
Human CDKL5 isoform 1 (CDKL5)	Dr. V. Kalscheuer, Max Planck Institute for Molecular Genetics, DE	N/A
mCerC1	(Gordon and Cousin, 2013)	N/A
mCer-hCDKL5 isoform 1	This paper	N/A
mCer-hCDKL5 K42R isoform 1	This paper	N/A
mCer-hCDKL5 R178P isoform 1	This paper	N/A
mCer-hCDKL5 ΔC isoform 1	This paper	N/A
mCer-hCDKL5 Δkinase isoform 1	This paper	N/A
pGEX-KG	Dr. C. Rickman, Heriot-Watt University, UK	N/A
Rat Amph1	Dr. H. T. McMahon, MRC Laboratory of Molecular Biology, UK	N/A
Syp1-mCer	(Gordon et al., 2011)	N/A
sypHy	Prof. L. Lagnado, University of Sussex	RRID:Addgene_24478
Software and Algorithms		
ACD/ChemSketch 2021.1.0	ACD/Labs	RRID:SCR_019272
Adobe Illustrator	Adobe Inc.	RRID:SCR_010279
Fiji ImageJ	https://imagej.net/software/fiji/	RRID:SCR_002285
GraphPad Prism 8.4.2	GraphPad Software Inc.	RRID:SCR_002798
Image Studio Lite Ver 5.2	LI-COR Biosciences	RRID:SCR_013715

Resource Availability

Lead Contact

Further information and requests for resources and reagents should be directed to and will be fulfilled by the Lead Contact, Michael Cousin (m.cousin@ed.ac.uk).

Materials Availability

All unique/stable reagents generated in this study are available from the Lead Contact without restriction.

Data and Code Availability

This study did not generate datasets/code.

EXPERIMENTAL MODEL AND SUBJECT DETAILS

Rats. All experimental procedures were conducted according to the UK Animal (Scientific Procedures) Act 1986 on the protection of animals used for scientific purposes and were

448 approved by the Animal Welfare and Ethical Review Body at the University of Edinburgh
449 (Home Office project license to M. Cousin – 7008878 or D. Wyllie - P1351480E). Adult animals
450 were killed by exposure to increasing CO_2 concentration followed by cervical dislocation,
451 while embryos were killed by decapitation followed by destruction of the brain. All animals
452 were maintained on a 12-hour light/dark cycle under constant temperature, with food and
453 water provided when needed.

454 *Cdkl5* KO Long-Evans rats were generated by Horizon Discovery, USA, following a CRISPR
455 interference approach to delete 10 bp in exon 8 of the *Cdkl5* gene (138367-76 in genomic
456 sequence) that results in the introduction of an early stop codon (Simões de Oliveira et al.
457 2022). *Cdkl5* heterozygous females (*Cdkl5*$^{+/-}$) were crossed with WT Long-Evans males
458 (*Cdkl5*$^{+/y}$) and the offspring were obtained from pregnant females at E17-E19. Prior to
459 genotyping, embryos were sexed by dissecting the abdomen to reveal their inner
460 reproductive organs. Male *Cdkl5*$^{-/y}$ embryos (referred to as CDKL5 KO) and male WT littermate
461 controls were used for neuronal cultures. WT and CDKL5 KO adult (> 2 months old) male rats
462 were used for biochemistry experiments. For CV analysis, primary hippocampal cultures were
463 prepared from WT mouse embryos (C57BL/6J) at E16-18.

464 **Genotyping.** Genomic DNA was obtained from nose or tail biopsies of embryos with alkaline
465 reagent containing 25 mM NaOH and 0.2 mM disodium EDTA (pH 12) at 95 °C (HotSHOT).
466 DNA extract (1 µl) was used for genotyping with the following primers (Eurogentec, BE): 5'-
467 GGGCTTGTAGCAAATCCATCC-3' (sense), 5'-ATACGTGGCTACTCGGTGGTAC-3' (sense;
468 matching 10 bp deletion), and 5'-AGCAAGCAGAGTTCTATTTTCCT-3' (antisense) using
469 polymerase chain reaction.

470 **METHOD DETAILS**

471 **DNA constructs.** The plasmid DNA vectors in this study were obtained as follows: sypHy from
472 Prof. L. Lagnado (University of Sussex, UK), full-length human CDKL5_1 (hCDKL5_1; referred
473 to as CDKL5) from Dr. V. Kalscheuer (Max Planck Institute for Molecular Genetics, Berlin,
474 Germany), full-length rat Amph1 from Dr. H. T. McMahon (MRC Laboratory of Molecular
475 Biology, Cambridge, UK), and pGEX-KG from Dr. C. Rickman (Heriot-Watt University,
476 Edinburgh, UK).

477 mCerulean (mCer)-C1-CDKL5 was generated by subcloning CDKL5 into an mCerC1 vector,
478 where the original GFP moiety was replaced by mCer (Gordon and Cousin, 2013), with the
479 primers 5'-CATCATCTCGAGGAATGAAGATTCCTAACATTGGTAATG-3' (sense) and 5'-
480 CATCATGGTACCTTACAAGGCTGTCTCTTTTAAATC-3' (antisense) with restriction sites
481 underlined. Deletion mutants of CDKL5 were generated using the subsequent primers: 5'-
482 CATCATCTCGAGTAATGAAGATTCCTAACATTGG-3' (sense) and 5'-
483 ATGATGGAATTCCTAAAATGTAGGGTGATTCAAAC-3' (antisense) for the kinase domain
484 (residues 1-297) and 5'-CATCATCTCGAGTACAAACCCAGAGACTTCTGG-3' (sense) and 5'-
485 ATGATGGGTACCTTACAAGGCTGTCTCTTTTAAATC-3' (antisense) for the C-terminal tail
486 (residues 298-960) with restriction sites underlined. Point mutations were introduced into
487 CDKL5 using standard site-directed mutagenesis protocols with the following primers: 5'-
488 GAAATTGTGGCGATCCGGAAATTCAAGGACAGT-3' (sense) and 5'-
489 ACTGTCCTTGAATTTCCGGATCGCCACAATTTC-3' (antisense) for K42R and 5'-

490 GCCACCAGATGGTATCCGTCCCCAGAACTCTTA-3' (sense) and 5'-
491 TAAGAGTTCTGGGGACGGATACCATCTGGTGGC-3' (antisense) for R178P with mutated sites
492 underlined. GST-Amph1 was generated by subcloning Amph1 (residues 248-620) into a pGEX-
493 KG vector using the primers 5'-CATCATGAATTCTAGGAGCTCCCAGTGATTCGGGTC-3' (sense)
494 and 5'-ATGATGCTCGAGCTAAGGAGGCAGTTCCTGAGCGG-3' (antisense) with restriction sites
495 underlined. Point mutations were introduced into Amph1 using standard site-directed
496 mutagenesis protocols with the following primers: 5'-
497 CCAGTGCGACCCAGAGCACCTTCACAGACAAGG-3' (sense) and 5'-
498 CCTTGTCTGTGAAGGTGCTCTGGGTCGCACTGG-3' (antisense) for S293A and 5'-
499 CCAGTGCGACCCAGAGAACCTTCACAGACAAGG-3' (sense) and 5'-
500 CCTTGTCTGTGAAGGTTCTCTGGGTCGCACTGG-3' (antisense) for S293E with mutated sites
501 underlined. All constructs were validated by Sanger sequencing.

502 **Neuronal cultures and transfection.** Hippocampi were dissected from CDKL5 KO male
503 embryos and littermate controls and dissociated in papain (10.5 U/ml). Tissue was triturated
504 in Dulbecco's Modified Eagle Medium/Nutrient Mixture F-12 supplemented with 10 % (v/v)
505 foetal bovine serum. Following a low-speed centrifugation, neurons were resuspended in
506 Neurobasal medium supplemented with 0.5 mM L-glutamine, 1 % (v/v) B27 supplement, and
507 penicillin/streptomycin. Neurons were plated on poly-D-lysine- and laminin-precoated
508 coverslips and kept in supplemented Neurobasal medium in a humidified incubator at 37 °C/5
509 % CO_2 for up to 15 days. Cytosine β-D-arabinofuranoside was added to neurons at 1 µM on 3
510 DIV to prevent glial proliferation. Neurons were transfected after 8-9 DIV with Lipofectamine
511 2000 as per manufacturer's instructions.

512 **Live-cell imaging and data analysis.** Primary hippocampal neurons at 13-15 DIV were
513 mounted in a closed bath imaging chamber (RC-21BRFS, Warner) allowing electrical field
514 stimulation (1-ms pulse width, 100 mA current output). Tyrode's buffer (119 mM NaCl, 2.5
515 mM KCl, 2 mM $CaCl_2$, 2 mM $MgCl_2$, 25 mM HEPES, 30 mM glucose, pH 7.4), supplemented
516 with 10 µM 6-cyano-7-nitroquinoxaline-2,3-dione (CNQX) and 50 µM DL-2-amino-5-
517 phosphonopentanoic acid (AP5) was perfused continuously. At the end of each recording,
518 neurons were perfused with 50 mM NH_4Cl solution, pH 7.4, substituting equal concentration
519 of NaCl in Tyrode's buffer. All recordings were performed at room temperature. Transfected
520 neurons were visualized using a Zeiss Axio Observer D1 inverted epifluorescence microscope
521 (Zeiss Ltd., Germany) with a 40x 1.3 NA oil immersion objective. Time-lapse images were
522 acquired using a Hamamatsu Orca-ER camera and the acquisition rate was set at 4 s
523 constantly pre- and post-stimulation. Neurons expressing sypHy and mCer constructs were
524 imaged at 500 nm and 430 nm excitation, respectively, using a 525-nm dichroic and a 535-nm
525 emission filter. To measure exocytosis rate, Tyrode's buffer was supplement with 1 µM
526 bafilomycin A1. To measure acidification kinetics, HEPES was replaced by 25 mM 2-(N-
527 morpholino)ethanesulfonic acid in Tyrode's buffer and acquisition rate was set at 2 s.

528 Time-lapse stacks of images were analysed using the Fiji is just ImageJ (Fiji) software
529 (Schindelin et al., 2012; Schneider et al., 2012). These were initially aligned using the StackReg
530 plugin with Rigid Body transformation type (Thevenaz et al., 1998). Regions of interest of 0.8
531 µm in diameter were placed on presynaptic boutons responsive to stimulation. Fluorescence

532 intensity was measured for all image slices using the Times Series Analyzer
533 (https://bit.ly/3M5hWpb). The average $\Delta F/F_0$ was calculated for each coverslip were
534 normalised to the maximum fluorescence intensity either during stimulation or NH_4Cl
535 perfusion. A one-phase exponential fit was used to correct baseline for bleaching that was
536 subtracted from all time points. Distance to the baseline at fixed time (122 s after termination
537 of stimulation) was used as a measure of endocytosis speed. No background was subtracted.

538 **Immunocytochemistry.** Primary cultured hippocampal neurons were fixed with 4 % (w/v)
539 paraformaldehyde/PBS for 10 min and neutralized with 50 mM NH_4Cl/PBS for 10 min. After
540 washing with PBS, neurons were permeabilized in 0.1 % (v/v) Triton X-100, 1 % (w/v) bovine
541 serum albumin/PBS for 5 min and blocked in 1 % (w/v) bovine serum albumin/PBS for 30 min.
542 Following blocking, neurons were incubated with the appropriate dilution of primary
543 antibodies for 1-2 h at room temperature. Primary antibodies were used as follows: sheep
544 CDKL5 (1:200), chicken GFP (1:5000), rabbit SV2A (1:200), and guinea pig VGLUT1 (1:1000).
545 Alexa Fluor secondary antibodies (1:1000) were applied for 1-2 h at room temperature in the
546 dark.

547 Transfected neurons were visualized using a Zeiss Axio Observer Z1 inverted epifluorescence
548 microscope (Zeiss Ltd., Germany) and a 40x 1.3 NA oil immersion objective at 480 nm and 550
549 nm excitation wavelengths. Fluorescent light was detected at 500-552 nm and >565 nm using
550 a 495-nm and a 565-nm dichroic filter, respectively. Neurons expressing mCer-tagged
551 constructs were visualized at 480 nm excitation wavelength using the anti-GFP antibody
552 described above. Images were acquired using a Zeiss AxioCam 506 camera and Zeiss ZEN 2
553 software. Data analysis was performed using Fiji. To quantify endogenous CDKL5 expression,
554 regions of interest were drawn manually around GFP-expressing cell bodies and average
555 CDKL5 signal was calculated and normalised to that of untransfected cell bodies. Background
556 was subtracted in all cases. For counting bouton numbers, MaxEntropy thresholding was
557 applied and positive accumulations of 0.64-2.24 µm in diameter were counted using the
558 Analyze particles plugin (Kapur et al., 1985). The number of SV2A- and VGLUT1-positive
559 puncta was counted in (50 x 15) μm^2 selections along neuronal processes to eliminate the
560 influence of neuronal density variation between genotypes. For CV analysis, the mean GFP
561 fluorescence along an axonal segment of > 15 µm was divided by the standard deviation and
562 expressed as a percentage (Gordon and Cousin, 2013). The average CV value of five axonal
563 segments was calculated per field of view.

564 **Biochemical isolation of crude SVs.** The crude purification of SVs was performed as described
565 previously (Huttner et al., 1983). An adult rat brain was homogenized in ice-cold 0.32 M
566 sucrose, 5 mM EDTA (pH 7.4) after removing the cerebellum. The homogenate (H) was
567 centrifuged twice at 950 x *g* for 10 min at 4 °C and the supernatant was collected each time.
568 The combined supernatant (S1) was spun at 20,400 x *g* for 30 min at 4 °C. The pellet (P2)
569 represents the crude synaptosomal fraction. For crude isolation of SVs, the P2 fraction was
570 resuspended in ice-cold 0.32 M sucrose/EDTA and incubated with 1 M HEPES/NaOH solution
571 (pH 7.4) on ice for 30 min. After spinning at 32,900 x *g* for 20 min at 4 °C, the lysate pellet
572 (LP1) and lysate supernatant (LS1) were obtained. The supernatant was then centrifuged at
573 268,000 x *g* for 2 h at 4 °C to generate LS2 and LP2 fractions. The LP2 pellet that represents

574 the crude SV fraction was collected and resuspended in 40 mM sucrose. Aliquots of the
575 intermediate fractions were kept for analysis. The total protein amount of the samples was
576 measured by Bradford and their concentration was adjusted to 1 mg/ml prior to Western blot
577 analysis.

578 **Immunoprecipitation.** Adult rat brain was mechanically homogenized in buffer containing 50
579 mM HEPES (pH 7.5), 0.5 % (v/v) Triton X-100, 150 mM NaCl, 1 mM EDTA, 1 mM EGTA, 1 mM
580 phenylmethylsulfonyl fluoride, and protease inhibitor cocktail. The homogenate was
581 incubated for 1-2 h at 4 ^{o}C rotating and then centrifuged at 155,000 x *g* for 40 min at 4 ^{o}C. The
582 supernatant was collected and pre-cleaned with Protein G Agarose beads (Sigma-Aldrich) for
583 1-2 h at 4 ^{o}C rotating to enhance specificity and the total protein content was quantified by
584 Bradford assay. The brain lysate (equivalent to 2 mg of protein) was incubated with 2-4 µg of
585 the antibody of interest at 4 ^{o}C rotating overnight. Next, Protein G Agarose beads
586 (approximately 20 µl) were added to the antibody-containing brain lysates and left rotating
587 for 1-2 h at 4 ^{o}C prior to being centrifuged at low speed. The supernatant was then discarded
588 and after three washes in HEPES buffer, Laemmli sample buffer was added directly to the
589 beads followed by heating at 95 ^{o}C for 5 min. A random antibody against Eps15 Homology
590 Domain protein (EHD) was used as a control.

591 **Drug treatments.** Cyclosporin A, calyculin A, PD98059 and roscovitine were dissolved in
592 dimethyl sulfoxide (DMSO), whereas AP5, CNQX, PD98059 and EGCG in ultrapure water for
593 stock concentration. For all drug experiments, culture medium was replaced by
594 unsupplemented Neurobasal medium and neurons were treated with appropriate drug
595 dilution at 37 ^{o}C. The drugs were administered as follows: 10 µM cyclosporin A or 100 nM
596 calyculin A for phosphatase inhibition experiments, 50 µM AP5 and 10 µM CNQX for electrical
597 stimulation, 20 mM EGCG, 100 µM PD98059, and 50 µM roscovitine for kinase inhibition
598 experiments. Stimulation was performed at room temperature in the presence of drugs in
599 Tyrode's buffer prior to lysis with Laemmli buffer.

600 **Pull-down.** Glutathione S-transferase (GST)-fused proteins were expressed in *Escherichia coli*
601 BL21(DE3) cells in lysogeny broth medium containing ampicillin after induction with 1 mM
602 isopropyl β-D-1-thiogalactopyranoside. Induced bacterial cultures were spun at 5000 x *g* for
603 15 min at 4 ^{o}C and the pellets were resuspended in ice-cold buffer containing 10 mM Tris, 150
604 mM NaCl, 1 mM EDTA, pH 8, protease inhibitors and 1 mM phenylmethylsulfonyl fluoride.
605 Lysozyme (0.0675 µg/µl), 4 mM dithiothreitol, and 10 % (v/v) Triton X-100 were also added.
606 The cells were sonicated at 10 kHz and the clear lysates were spun at 17,420 x *g* for 10 min at
607 4 ^{o}C. The supernatant was transferred to pre-washed Glutathione Sepharose 4B beads
608 resuspended in PBS to create a 50 % suspension and left rotating overnight at 4 ^{o}C. A small
609 volume of glutathione -coupled GST-fused proteins was loaded into a ProbeQuant G-50 Micro
610 Column and washed once in ice cold lysis buffer containing 1 % (v/v) Triton X-100, 25 mM Tris-
611 HCl, 150 mM NaCl, 1 mM EGTA, 1 mM EDTA, pH 7.4, prior to incubation with synaptosomal
612 lysates. The columns were washed successively in ice cold lysis buffer, in NaCl-supplemented
613 lysis buffer (500 mM) and in 20 mM Tris, pH 7.4. Laemmli sample buffer was added into the
614 columns and the eluted proteins were denatured at 95 ^{o}C for 5 min. All GST-coupled Amph1
615 constructs were devoid of the N-terminal Bin/Amphiphysin/Rvs (N-BAR) and the Src-

homology 3 (SH3) domains and their total level was estimated with Coomassie Brilliant blue staining prior to Western blot analysis.

Western blotting. Brain samples were prepared as described above, whereas hippocampal neurons at 14-15 DIV were lysed directly with Laemmli sample buffer. Proteins were denatured at 95 °C for 5 min. Protein extracts were separated by SDS-PAGE, transferred to a nitrocellulose membrane, and blocked in Intercept (PBS or TBS) blocking buffer. Membranes were incubated with primary antibodies at 4 °C overnight and IRDye secondary antibodies (1:10000) for 2 h at room temperature in Intercept (PBS or TBS) blocking buffer containing 0.1 % (v/v) Tween-20 in the dark. Blots were visualized using the LI-COR Biosciences Odyssey Infrared Imaging System and quantification of band densities was performed using the Image Studio Lite version 5.2 software with background subtraction or Fiji. Equal protein amount loading was verified by Ponceau-S staining. The primary (phospho)antibodies that were used in this study are: sheep CDKL5 (1:500), goat Amph1 (1:500), goat CHC (1:250), goat syndapin 1 (1:1000), guinea pig VGLUT1 (1:2000), rabbit ATP6V1B2 (1:5000), goat Dyn1 (1:500), rabbit Syp1 (1:500), mouse PSD95 (1:1000), mouse β-actin-peroxidase (1:30000), rabbit pMAP1S-S900 (light chain) (1:50), sheep pDyn1-S774 (1:1000), rabbit pAkt-S473 (1:1000), rabbit pGSK3α/β-S9/S21 (1:1000). For experiments assessing the phosphorylation levels of Amph1-S293, a rabbit polyclonal phosphoantibody was raised against the peptide PVRPRS^{293}PSQTRC of Amph1 (0.5 mg/ml).

Statistical analysis and experimental design. Statistical calculations were conducted using GraphPad Prism 8.4.2 (GraphPad Software Inc). The normality of the data distribution was assessed by performing D'Agostino and Pearson omnibus normality test with significance level set at $\alpha = 0.05$. Datasets following a Gaussian distribution were presented as mean ± standard error of the mean (SEM) and statistical significance was assessed by two-tailed unpaired t test for comparison between two groups or analysis of variance (ANOVA) followed by Tukey's, Dunnett's or Sidak's post hoc analysis for multiple comparisons. Datasets following a non-Gaussian distribution were presented as median with interquartile range (IQR) indicating min to max whiskers and statistical significance was evaluated by Mann-Whitney test for comparison between two groups or Kruskal-Wallis followed by Dunn's post hoc analysis for multiple comparisons. For experiments with a small number of replicates for a normality test to be performed, a parametric test was assumed. Asterisks refer to *p*-values as follows: *; $p \leq 0.05$, **; $p \leq 0.005$, ***; $p \leq 0.001$, ****; $p \leq 0.0001$. All experiments consisted of at least three independent biological replicates. Live-imaging data were analysed blind for experiments consisting of two groups. Random variation or effect size were not estimated. Sample size and statistical test are indicated in the figure legends. Detailed description of the statistical tests and p values are presented in **Table S1**.

652 **References**

653 Amendola, E., Zhan, Y., Mattucci, C., Castroflorio, E., Calcagno, E., Fuchs, C., Lonetti, G.,
654 Silingardi, D., Vyssotski, A.L., Farley, D., et al. (2014). Mapping pathological phenotypes in a
655 mouse model of CDKL5 disorder. PLoS One *9*, e91613. 10.1371/journal.pone.0091613.

656 Atluri, P.P., and Ryan, T.A. (2006). The kinetics of synaptic vesicle reacidification at
657 hippocampal nerve terminals. J Neurosci *26*, 2313-2320. 10.1523/JNEUROSCI.4425-05.2006.

658 Baker, K., Gordon, S.L., Melland, H., Bumbak, F., Scott, D.J., Jiang, T.J., Owen, D., Turner, B.J.,
659 Boyd, S.G., Rossi, M., et al. (2018). SYT1-associated neurodevelopmental disorder: a case
660 series. Brain *141*, 2576-2591. 10.1093/brain/awy209.

661 Baltussen, L.L., Negraes, P.D., Silvestre, M., Claxton, S., Moeskops, M., Christodoulou, E.,
662 Flynn, H.R., Snijders, A.P., Muotri, A.R., and Ultanir, S.K. (2018). Chemical genetic
663 identification of CDKL5 substrates reveals its role in neuronal microtubule dynamics. EMBO J
664 *37*. 10.15252/embj.201899763.

665 Bartos, M., Vida, I., and Jonas, P. (2007). Synaptic mechanisms of synchronized gamma
666 oscillations in inhibitory interneuron networks. Nat Rev Neurosci *8*, 45-56. 10.1038/nrn2044.

667 Bauerfeind, R., Takei, K., and De Camilli, P. (1997). Amphiphysin I is associated with coated
668 endocytic intermediates and undergoes stimulation-dependent dephosphorylation in nerve
669 terminals. J Biol Chem *272*, 30984-30992. 10.1074/jbc.272.49.30984.

670 Boumil, R.M., Letts, V.A., Roberts, M.C., Lenz, C., Mahaffey, C.L., Zhang, Z.W., Moser, T., and
671 Frankel, W.N. (2010). A missense mutation in a highly conserved alternate exon of dynamin-
672 1 causes epilepsy in fitful mice. PLoS Genet *6*. 10.1371/journal.pgen.1001046.

673 Clayton, E.L., Anggono, V., Smillie, K.J., Chau, N., Robinson, P.J., and Cousin, M.A. (2009). The
674 phospho-dependent dynamin-syndapin interaction triggers activity-dependent bulk
675 endocytosis of synaptic vesicles. J Neurosci *29*, 7706-7717. 10.1523/JNEUROSCI.1976-
676 09.2009.

677 Clayton, E.L., Sue, N., Smillie, K.J., O'Leary, T., Bache, N., Cheung, G., Cole, A.R., Wyllie, D.J.,
678 Sutherland, C., Robinson, P.J., and Cousin, M.A. (2010). Dynamin I phosphorylation by GSK3
679 controls activity-dependent bulk endocytosis of synaptic vesicles. Nat Neurosci *13*, 845-851.
680 10.1038/nn.2571.

681 Cousin, M.A. (2017). Integration of Synaptic Vesicle Cargo Retrieval with Endocytosis at
682 Central Nerve Terminals. Front Cell Neurosci *11*, 234. 10.3389/fncel.2017.00234.

683 Cousin, M.A., and Robinson, P.J. (2001). The dephosphins: dephosphorylation by calcineurin
684 triggers synaptic vesicle endocytosis. Trends Neurosci *24*, 659-665. 10.1016/s0166-
685 2236(00)01930-5.

686 Craft, G.E., Graham, M.E., Bache, N., Larsen, M.R., and Robinson, P.J. (2008). The in vivo
687 phosphorylation sites in multiple isoforms of amphiphysin I from rat brain nerve terminals.
688 Mol Cell Proteomics *7*, 1146-1161. 10.1074/mcp.M700351-MCP200.

689 Della Sala, G., Putignano, E., Chelini, G., Melani, R., Calcagno, E., Michele Ratto, G., Amendola,
690 E., Gross, C.T., Giustetto, M., and Pizzorusso, T. (2016). Dendritic Spine Instability in a Mouse
691 Model of CDKL5 Disorder Is Rescued by Insulin-like Growth Factor 1. Biol Psychiatry *80*, 302-
692 311. 10.1016/j.biopsych.2015.08.028.

693 Dhindsa, R.S., Bradrick, S.S., Yao, X., Heinzen, E.L., Petrovski, S., Krueger, B.J., Johnson, M.R.,
694 Frankel, W.N., Petrou, S., Boumil, R.M., and Goldstein, D.B. (2015). Epileptic encephalopathy-
695 causing mutations in DNM1 impair synaptic vesicle endocytosis. Neurol Genet *1*, e4.
696 10.1212/01.NXG.0000464295.65736.da.

697 Di Paolo, G., Sankaranarayanan, S., Wenk, M.R., Daniell, L., Perucco, E., Caldarone, B.J., Flavell,
698 R., Picciotto, M.R., Ryan, T.A., Cremona, O., and De Camilli, P. (2002). Decreased synaptic
699 vesicle recycling efficiency and cognitive deficits in amphiphysin 1 knockout mice. Neuron *33*,
700 789-804. 10.1016/s0896-6273(02)00601-3.

701 Egashira, Y., Takase, M., and Takamori, S. (2015). Monitoring of vacuolar-type H+ ATPase-
702 mediated proton influx into synaptic vesicles. J Neurosci *35*, 3701-3710.
703 10.1523/JNEUROSCI.4160-14.2015.

704 Elia, M., Falco, M., Ferri, R., Spalletta, A., Bottitta, M., Calabrese, G., Carotenuto, M.,
705 Musumeci, S.A., Lo Giudice, M., and Fichera, M. (2008). CDKL5 mutations in boys with severe
706 encephalopathy and early-onset intractable epilepsy. Neurology *71*, 997-999.
707 10.1212/01.wnl.0000326592.37105.88.

708 Fassio, A., Esposito, A., Kato, M., Saitsu, H., Mei, D., Marini, C., Conti, V., Nakashima, M.,
709 Okamoto, N., Olmez Turker, A., et al. (2018). De novo mutations of the ATP6V1A gene cause
710 developmental encephalopathy with epilepsy. Brain *141*, 1703-1718. 10.1093/brain/awy092.

711 Fehr, S., Wilson, M., Downs, J., Williams, S., Murgia, A., Sartori, S., Vecchi, M., Ho, G., Polli, R.,
712 Psoni, S., et al. (2013). The CDKL5 disorder is an independent clinical entity associated with
713 early-onset encephalopathy. Eur J Hum Genet *21*, 266-273. 10.1038/ejhg.2012.156.

714 Ferreira, A.P.A., Casamento, A., Carrillo Roas, S., Halff, E.F., Panambalana, J., Subramaniam,
715 S., Schutzenhofer, K., Chan Wah Hak, L., McGourty, K., Thalassinos, K., et al. (2021). Cdk5 and
716 GSK3beta inhibit fast endophilin-mediated endocytosis. Nat Commun *12*, 2424.
717 10.1038/s41467-021-22603-4.

718 Floyd, S., Porro, E.B., Slepnev, V.I., Ochoa, G.C., Tsai, L.H., and De Camilli, P. (2001).
719 Amphiphysin 1 binds the cyclin-dependent kinase (cdk) 5 regulatory subunit p35 and is
720 phosphorylated by cdk5 and cdc2. J Biol Chem *276*, 8104-8110. 10.1074/jbc.M008932200.

721 Gordon, S.L., and Cousin, M.A. (2013). X-linked intellectual disability-associated mutations in
722 synaptophysin disrupt synaptobrevin II retrieval. J Neurosci *33*, 13695-13700.
723 10.1523/JNEUROSCI.0636-13.2013.

724 Gordon, S.L., Leube, R.E., and Cousin, M.A. (2011). Synaptophysin is required for
725 synaptobrevin retrieval during synaptic vesicle endocytosis. J Neurosci *31*, 14032-14036.
726 10.1523/JNEUROSCI.3162-11.2011.

727 Granseth, B., Odermatt, B., Royle, S.J., and Lagnado, L. (2006). Clathrin-mediated endocytosis
728 is the dominant mechanism of vesicle retrieval at hippocampal synapses. Neuron *51*, 773-786.
729 10.1016/j.neuron.2006.08.029.

730 Hector, R.D., Kalscheuer, V.M., Hennig, F., Leonard, H., Downs, J., Clarke, A., Benke, T.A.,
731 Armstrong, J., Pineda, M., Bailey, M.E.S., and Cobb, S.R. (2017). CDKL5 variants: Improving our
732 understanding of a rare neurologic disorder. Neurol Genet *3*, e200.
733 10.1212/NXG.0000000000000200.

734 Huttner, W.B., Schiebler, W., Greengard, P., and De Camilli, P. (1983). Synapsin I (protein I), a
735 nerve terminal-specific phosphoprotein. III. Its association with synaptic vesicles studied in a
736 highly purified synaptic vesicle preparation. J Cell Biol *96*, 1374-1388. 10.1083/jcb.96.5.1374.

737 Jiang, Z., Gong, T., and Wei, H. (2019). CDKL5 promotes proliferation, migration, and
738 chemotherapeutic drug resistance of glioma cells via activation of the PI3K/AKT signaling
739 pathway. FEBS Open Bio. 10.1002/2211-5463.12780.

740 Kapur, J.N., Sahoo, P.K., and Wong, A.K.C. (1985). A New Method for Gray-Level Picture
741 Thresholding Using the Entropy of the Histogram. Comput Vision Graph *29*, 273-285. Doi
742 10.1016/0734-189x(85)90125-2.

743 Katayama, S., Sueyoshi, N., and Kameshita, I. (2015). Critical Determinants of Substrate
744 Recognition by Cyclin-Dependent Kinase-like 5 (CDKL5). Biochemistry *54*, 2975-2987.
745 10.1021/bi501308k.

746 Kilstrup-Nielsen, C., Rusconi, L., La Montanara, P., Ciceri, D., Bergo, A., Bedogni, F., and
747 Landsberger, N. (2012). What we know and would like to know about CDKL5 and its
748 involvement in epileptic encephalopathy. Neural Plast *2012*, 728267. 10.1155/2012/728267.

749 Kim, Y., Park, J., Song, W.J., and Chang, S. (2010). Overexpression of Dyrk1A causes the defects
750 in synaptic vesicle endocytosis. Neurosignals *18*, 164-172. 10.1159/000321994.

751 Kind, P.C., and Bird, A. (2021). CDKL5 deficiency disorder: a pathophysiology of neural
752 maintenance. J Clin Invest *131*. 10.1172/JCI153606.

753 Koch, D., Spiwoks-Becker, I., Sabanov, V., Sinning, A., Dugladze, T., Stellmacher, A., Ahuja, R.,
754 Grimm, J., Schuler, S., Muller, A., et al. (2011). Proper synaptic vesicle formation and neuronal
755 network activity critically rely on syndapin I. EMBO J *30*, 4955-4969.
756 10.1038/emboj.2011.339.

757 Liang, S., Wei, F.Y., Wu, Y.M., Tanabe, K., Abe, T., Oda, Y., Yoshida, Y., Yamada, H., Matsui, H.,
758 Tomizawa, K., and Takei, K. (2007). Major Cdk5-dependent phosphorylation sites of
759 amphiphysin 1 are implicated in the regulation of the membrane binding and endocytosis. J
760 Neurochem *102*, 1466-1476. 10.1111/j.1471-4159.2007.04507.x.

761 Lin, C., Franco, B., and Rosner, M.R. (2005). CDKL5/Stk9 kinase inactivation is associated with
762 neuronal developmental disorders. Hum Mol Genet *14*, 3775-3786. 10.1093/hmg/ddi391.

763 Liu, J.P., Sim, A.T., and Robinson, P.J. (1994). Calcineurin inhibition of dynamin I GTPase
764 activity coupled to nerve terminal depolarization. Science *265*, 970-973.
765 10.1126/science.8052858.

766 Marks, B., and McMahon, H.T. (1998). Calcium triggers calcineurin-dependent synaptic vesicle
767 recycling in mammalian nerve terminals. Curr Biol *8*, 740-749. 10.1016/s0960-
768 9822(98)70297-0.

769 McAdam, R.L., Morton, A., Gordon, S.L., Alterman, J.F., Khvorova, A., Cousin, M.A., and Smillie,
770 K.J. (2020). Loss of huntingtin function slows synaptic vesicle endocytosis in striatal neurons
771 from the htt(Q140/Q140) mouse model of Huntington's disease. Neurobiol Dis *134*, 104637.
772 10.1016/j.nbd.2019.104637.

773 Micheva, K.D., Ramjaun, A.R., Kay, B.K., and McPherson, P.S. (1997). SH3 domain-dependent
774 interactions of endophilin with amphiphysin. FEBS Lett *414*, 308-312. 10.1016/s0014-
775 5793(97)01016-8.

776 Miesenbock, G., De Angelis, D.A., and Rothman, J.E. (1998). Visualizing secretion and synaptic
777 transmission with pH-sensitive green fluorescent proteins. Nature *394*, 192-195.
778 10.1038/28190.

779 Munoz, I.M., Morgan, M.E., Peltier, J., Weiland, F., Gregorczyk, M., Brown, F.C., Macartney,
780 T., Toth, R., Trost, M., and Rouse, J. (2018). Phosphoproteomic screening identifies
781 physiological substrates of the CDKL5 kinase. EMBO J *37*. 10.15252/embj.201899559.

782 Murakami, N., Xie, W., Lu, R.C., Chen-Hwang, M.C., Wieraszko, A., and Hwang, Y.W. (2006).
783 Phosphorylation of amphiphysin I by minibrain kinase/dual-specificity tyrosine
784 phosphorylation-regulated kinase, a kinase implicated in Down syndrome. J Biol Chem *281*,
785 23712-23724. 10.1074/jbc.M513497200.

786 Nawaz, M.S., Giarda, E., Bedogni, F., La Montanara, P., Ricciardi, S., Ciceri, D., Alberio, T.,
787 Landsberger, N., Rusconi, L., and Kilstrup-Nielsen, C. (2016). CDKL5 and Shootin1 Interact and
788 Concur in Regulating Neuronal Polarization. PLoS One *11*, e0148634.
789 10.1371/journal.pone.0148634.

790 Nemos, C., Lambert, L., Giuliano, F., Doray, B., Roubertie, A., Goldenberg, A., Delobel, B.,
791 Layet, V., N'Guyen M, A., Saunier, A., et al. (2009). Mutational spectrum of CDKL5 in early-
792 onset encephalopathies: a study of a large collection of French patients and review of the
793 literature. Clin Genet *76*, 357-371. 10.1111/j.1399-0004.2009.01194.x.

794 Nichols, R.A., Suplick, G.R., and Brown, J.M. (1994). Calcineurin-mediated protein
795 dephosphorylation in brain nerve terminals regulates the release of glutamate. J Biol Chem
796 *269*, 23817-23823.

797 Oi, A., Katayama, S., Hatano, N., Sugiyama, Y., Kameshita, I., and Sueyoshi, N. (2017).
798 Subcellular distribution of cyclin-dependent kinase-like 5 (CDKL5) is regulated through
799 phosphorylation by dual specificity tyrosine-phosphorylation-regulated kinase 1A (DYRK1A).
800 Biochem Biophys Res Commun *482*, 239-245. 10.1016/j.bbrc.2016.11.048.

801 Okuda, K., Kobayashi, S., Fukaya, M., Watanabe, A., Murakami, T., Hagiwara, M., Sato, T.,
802 Ueno, H., Ogonuki, N., Komano-Inoue, S., et al. (2017). CDKL5 controls postsynaptic
803 localization of GluN2B-containing NMDA receptors in the hippocampus and regulates seizure
804 susceptibility. Neurobiol Dis *106*, 158-170. 10.1016/j.nbd.2017.07.002.

805 Parenti, I., Rabaneda, L.G., Schoen, H., and Novarino, G. (2020). Neurodevelopmental
806 Disorders: From Genetics to Functional Pathways. Trends Neurosci *43*, 608-621.
807 10.1016/j.tins.2020.05.004.

808 Ren, E., Roncace, V., Trazzi, S., Fuchs, C., Medici, G., Gennaccaro, L., Loi, M., Galvani, G., Ye,
809 K., Rimondini, R., et al. (2019). Functional and Structural Impairments in the Perirhinal Cortex
810 of a Mouse Model of CDKL5 Deficiency Disorder Are Rescued by a TrkB Agonist. Front Cell
811 Neurosci *13*, 169. 10.3389/fncel.2019.00169.

812 Ricciardi, S., Ungaro, F., Hambrock, M., Rademacher, N., Stefanelli, G., Brambilla, D., Sessa, A.,
813 Magagnotti, C., Bachi, A., Giarda, E., et al. (2012). CDKL5 ensures excitatory synapse stability
814 by reinforcing NGL-1-PSD95 interaction in the postsynaptic compartment and is impaired in
815 patient iPSC-derived neurons. Nat Cell Biol *14*, 911-923. 10.1038/ncb2566.

816 Rusconi, L., Kilstrup-Nielsen, C., and Landsberger, N. (2011). Extrasynaptic N-methyl-D-
817 aspartate (NMDA) receptor stimulation induces cytoplasmic translocation of the CDKL5
818 kinase and its proteasomal degradation. J Biol Chem *286*, 36550-36558.
819 10.1074/jbc.M111.235630.

820 Salpietro, V., Malintan, N.T., Llano-Rivas, I., Spaeth, C.G., Efthymiou, S., Striano, P.,
821 Vandrovcova, J., Cutrupi, M.C., Chimenz, R., David, E., et al. (2019). Mutations in the Neuronal
822 Vesicular SNARE VAMP2 Affect Synaptic Membrane Fusion and Impair Human
823 Neurodevelopment. Am J Hum Genet *104*, 721-730. 10.1016/j.ajhg.2019.02.016.

824 Sankaranarayanan, S., and Ryan, T.A. (2000). Real-time measurements of vesicle-SNARE
825 recycling in synapses of the central nervous system. Nat Cell Biol *2*, 197-204.
826 10.1038/35008615.

827 Sankaranarayanan, S., and Ryan, T.A. (2001). Calcium accelerates endocytosis of vSNAREs at
828 hippocampal synapses. Nat Neurosci *4*, 129-136. 10.1038/83949.

829 Schindelin, J., Arganda-Carreras, I., Frise, E., Kaynig, V., Longair, M., Pietzsch, T., Preibisch, S.,
830 Rueden, C., Saalfeld, S., Schmid, B., et al. (2012). Fiji: an open-source platform for biological-
831 image analysis. Nat Methods *9*, 676-682. 10.1038/nmeth.2019.

832 Schneider, C.A., Rasband, W.S., and Eliceiri, K.W. (2012). NIH Image to ImageJ: 25 years of
833 image analysis. Nat Methods *9*, 671-675. 10.1038/nmeth.2089.

834 Schroeder, E., Yuan, L., Seong, E., Ligon, C., DeKorver, N., Gurumurthy, C.B., and Arikkath, J.
835 (2019). Neuron-Type Specific Loss of CDKL5 Leads to Alterations in mTOR Signaling and
836 Synaptic Markers. Mol Neurobiol *56*, 4151-4162. 10.1007/s12035-018-1346-8.

837 Sekiguchi, M., Katayama, S., Hatano, N., Shigeri, Y., Sueyoshi, N., and Kameshita, I. (2013).
838 Identification of amphiphysin 1 as an endogenous substrate for CDKL5, a protein kinase

839 associated with X-linked neurodevelopmental disorder. Arch Biochem Biophys *535*, 257-267.
840 10.1016/j.abb.2013.04.012.

841 Serajee, F.J., and Huq, A.M. (2015). Homozygous Mutation in Synaptic Vesicle Glycoprotein
842 2A Gene Results in Intractable Epilepsy, Involuntary Movements, Microcephaly, and
843 Developmental and Growth Retardation. Pediatr Neurol *52*, 642-646 e641.
844 10.1016/j.pediatrneurol.2015.02.011.

845 Shang, W.H., Adachi, Y., Nakamura, A., Copeland, T., Kim, S.R., and Kamata, T. (2004).
846 Regulation of amphiphysin1 by mitogen-activated protein kinase: its significance in nerve
847 growth factor receptor-mediated endocytosis. J Biol Chem *279*, 40890-40896.
848 10.1074/jbc.M404527200.

849 Simões de Oliveira, L., O'Leary, H.E., Nawaz, S., Lourerio, R., Davenport, E.C., Baxter, P., Dando,
850 O.R., Perkins, E., Booker, S.A., Hardingham, G.E., et al. (2022)
851 bioRxiv 2022.06.29.497927; doi: https://doi.org/10.1101/2022.06.29.497927

852 Sivilia, S., Mangano, C., Beggiato, S., Giuliani, A., Torricella, R., Baldassarro, V.A., Fernandez,
853 M., Lorenzini, L., Giardino, L., Borelli, A.C., et al. (2016). CDKL5 knockout leads to altered
854 inhibitory transmission in the cerebellum of adult mice. Genes Brain Behav *15*, 491-502.
855 10.1111/gbb.12292.

856 Smillie, K.J., and Cousin, M.A. (2012). Akt/PKB controls the activity-dependent bulk
857 endocytosis of synaptic vesicles. Traffic *13*, 1004-1011. 10.1111/j.1600-0854.2012.01365.x.

858 Soykan, T., Maritzen, T., and Haucke, V. (2016). Modes and mechanisms of synaptic vesicle
859 recycling. Curr Opin Neurobiol *39*, 17-23. 10.1016/j.conb.2016.03.005.

860 Tan, T.C., Valova, V.A., Malladi, C.S., Graham, M.E., Berven, L.A., Jupp, O.J., Hansra, G.,
861 McClure, S.J., Sarcevic, B., Boadle, R.A., et al. (2003). Cdk5 is essential for synaptic vesicle
862 endocytosis. Nat Cell Biol *5*, 701-710. 10.1038/ncb1020.

863 Tang, S., Terzic, B., Wang, I.J., Sarmiento, N., Sizov, K., Cui, Y., Takano, H., Marsh, E.D., Zhou,
864 Z., and Coulter, D.A. (2019). Altered NMDAR signaling underlies autistic-like features in mouse
865 models of CDKL5 deficiency disorder. Nat Commun *10*, 2655. 10.1038/s41467-019-10689-w.

866 Tang, S., Wang, I.J., Yue, C., Takano, H., Terzic, B., Pance, K., Lee, J.Y., Cui, Y., Coulter, D.A., and
867 Zhou, Z. (2017). Loss of CDKL5 in Glutamatergic Neurons Disrupts Hippocampal Microcircuitry
868 and Leads to Memory Impairment in Mice. J Neurosci *37*, 7420-7437.
869 10.1523/JNEUROSCI.0539-17.2017.

870 Terzic, B., Davatolhagh, M.F., Ho, Y., Tang, S., Liu, Y.T., Xia, Z., Cui, Y., Fuccillo, M.V., and Zhou,
871 Z. (2021). Temporal manipulation of Cdkl5 reveals essential postdevelopmental functions and
872 reversible CDKL5 deficiency disorder-related deficits. J Clin Invest *131*. 10.1172/JCI143655.

873 Thapar, A., Cooper, M., and Rutter, M. (2017). Neurodevelopmental disorders. Lancet
874 Psychiatry *4*, 339-346. 10.1016/S2215-0366(16)30376-5.

875 Thevenaz, P., Ruttimann, U.E., and Unser, M. (1998). A pyramid approach to subpixel
876 registration based on intensity. IEEE Trans Image Process *7*, 27-41. 10.1109/83.650848.

877 Trovo, L., Fuchs, C., De Rosa, R., Barbiero, I., Tramarin, M., Ciani, E., Rusconi, L., and Kilstrup-
878 Nielsen, C. (2020). The green tea polyphenol epigallocatechin-3-gallate (EGCG) restores
879 CDKL5-dependent synaptic defects in vitro and in vivo. Neurobiol Dis *138*, 104791.
880 10.1016/j.nbd.2020.104791.

881 Wang, H.T., Zhu, Z.A., Li, Y.Y., Lou, S.S., Yang, G., Feng, X., Xu, W., Huang, Z.L., Cheng, X., and
882 Xiong, Z.Q. (2021). CDKL5 deficiency in forebrain glutamatergic neurons results in recurrent
883 spontaneous seizures. Epilepsia *62*, 517-528. 10.1111/epi.16805.

884 Wang, I.T., Allen, M., Goffin, D., Zhu, X., Fairless, A.H., Brodkin, E.S., Siegel, S.J., Marsh, E.D.,
885 Blendy, J.A., and Zhou, Z. (2012). Loss of CDKL5 disrupts kinome profile and event-related
886 potentials leading to autistic-like phenotypes in mice. Proc Natl Acad Sci U S A *109*, 21516-
887 21521. 10.1073/pnas.1216988110.

888 Wigge, P., and McMahon, H.T. (1998). The amphiphysin family of proteins and their role in
889 endocytosis at the synapse. Trends Neurosci *21*, 339-344. 10.1016/s0166-2236(98)01264-8.

890 Wu, Y., Matsui, H., and Tomizawa, K. (2009). Amphiphysin I and regulation of synaptic vesicle
891 endocytosis. Acta Med Okayama *63*, 305-323. 10.18926/AMO/31822.

892 Yennawar, M., White, R.S., and Jensen, F.E. (2019). AMPA Receptor Dysregulation and
893 Therapeutic Interventions in a Mouse Model of CDKL5 Deficiency Disorder. J Neurosci *39*,
894 4814-4828. 10.1523/JNEUROSCI.2041-18.2019.

895 Zhao, H., Kim, Y., Park, J., Park, D., Lee, S.E., Chang, I., and Chang, S. (2014). SCAMP5 plays a
896 critical role in synaptic vesicle endocytosis during high neuronal activity. J Neurosci *34*, 10085-
897 10095. 10.1523/JNEUROSCI.2156-14.2014.

898 Zhu, Y.C., Li, D., Wang, L., Lu, B., Zheng, J., Zhao, S.L., Zeng, R., and Xiong, Z.Q. (2013).
899 Palmitoylation-dependent CDKL5-PSD-95 interaction regulates synaptic targeting of CDKL5
900 and dendritic spine development. Proc Natl Acad Sci U S A *110*, 9118-9123.
901 10.1073/pnas.1300003110.

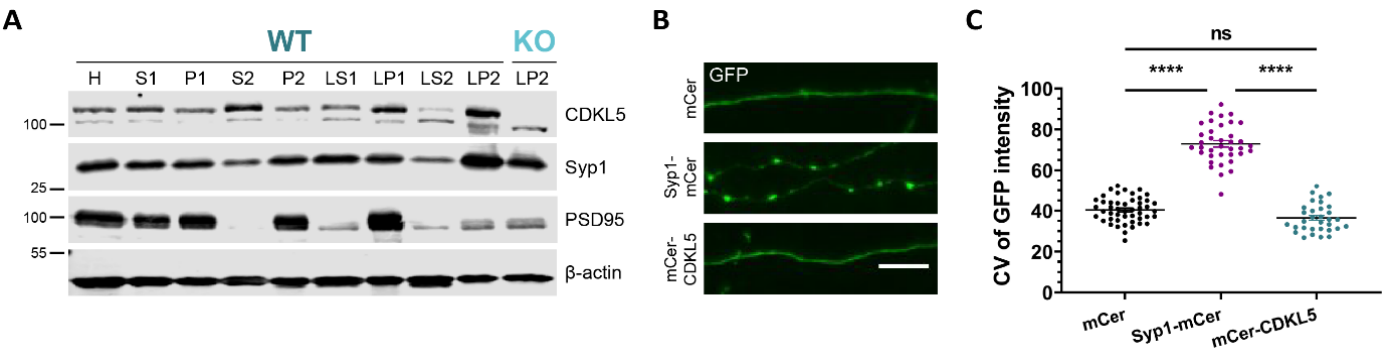

Figure 1. CDKL5 is present at nerve terminals. (*A*) Subcellular fractionation of adult rat brain for the crude purification of a synaptosomal (P2) and an SV (LP2) fraction and fractions representing other subcellular compartments (H, homogenate; P1, tissue debris, nuclei, and large myelin fragments; S2, microsomes, mitochondria, and synaptosomes; LP1, synaptic membrane, mitochondria, and myelin fragments; LS2, synaptosomal cytoplasm). An LP2 fraction from an adult CDKL5 KO rat brain was also generated. CDKL5 is enriched in the LP2 fraction (top band; 110 KDa). Synaptophysin 1 (Syp1) and postsynaptic density 95 (PSD95) were used as pre- and postsynaptic markers, respectively, and β-actin as loading control. (*B*) Mouse hippocampal neurons were transfected with either mCer, Syp1-mCer or mCer-CDKL5 at 8-9 DIV, fixed at 15 DIV, and stained for GFP. Examples of axonal segments of > 15 µm that were selected for coefficient of variation (CV) analysis are displayed. Scale bar, 5 µm. (*C*) The distribution pattern of CDKL5 was assessed by CV analysis of GFP fluorescence intensity along multiple > 15 µm axonal segments per field of view. Scatter plots indicate mean ± SEM. ns, not significant, ****$p < 0.0001$ by one-way ANOVA followed by Tukey's multiple comparison test. mCer $n = 48$, Syp1-mCer $n = 37$, mCer-CDKL5 $n = 32$ fields of view from 4 independent preparations of neuronal cultures.

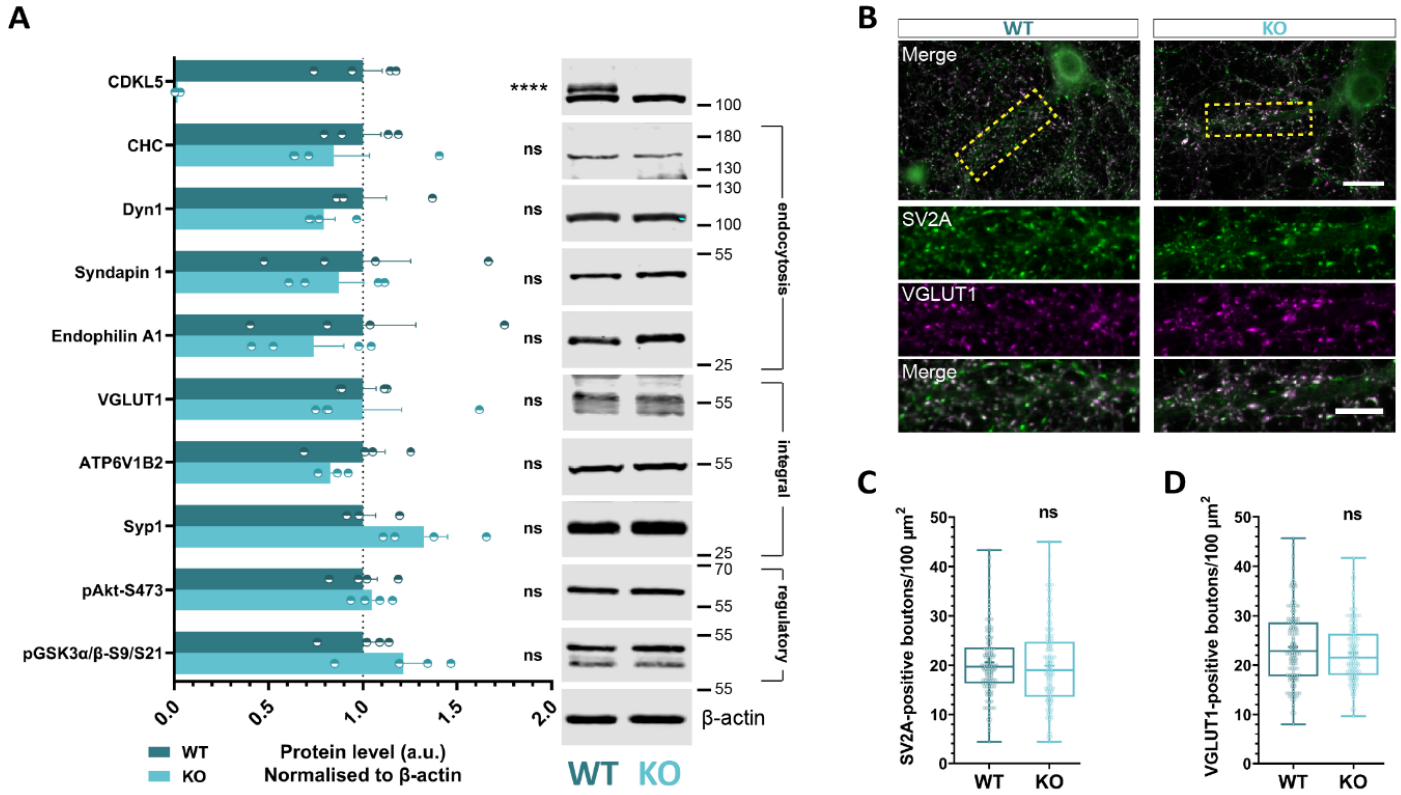

Figure 2. Loss of CDKL5 does not alter presynaptic protein levels or the number of presynaptic boutons. (*A*) Hippocampal neuronal lysates at 14-15 DIV were analysed for different presynaptic proteins, including SV endocytosis proteins, integral SV proteins, and phosphoproteins regulating SV endocytosis. Quantification of the total band intensity normalised to β-actin revealed no difference for any of these proteins in the absence of CDKL5. Bars indicate mean ± SEM. ns, not significant, ****$p < 0.0001$ by unpaired two-tailed t test. WT $n = 4$, KO $n = 4$ neuronal lysates from 4 independent preparations of neuronal cultures. (*B*) Hippocampal neuronal cultures derived from WT and CDKL5 KO rats were fixed at 15 DIV and stained for the presynaptic proteins SV2A and VGLUT1. The number of positive puncta was counted in (50 x 15) μm^2 selections along processes (dashed yellow boxes) for both markers. Scale bar, 20 µm (neurons), 10 µm (processes). (*C*) Quantification of SV2A-positive boutons and (*D*) VGLUT1-positive boutons per 100 μm^2 along WT and CDKL5 KO dendrites. Box plots present median with IQR indicating min to max whiskers. ns, not significant by Mann Whitney two-tailed t test, + indicates mean value. WT $n = 144$, KO $n = 142$ neurons from 3 independent preparations of neuronal cultures.

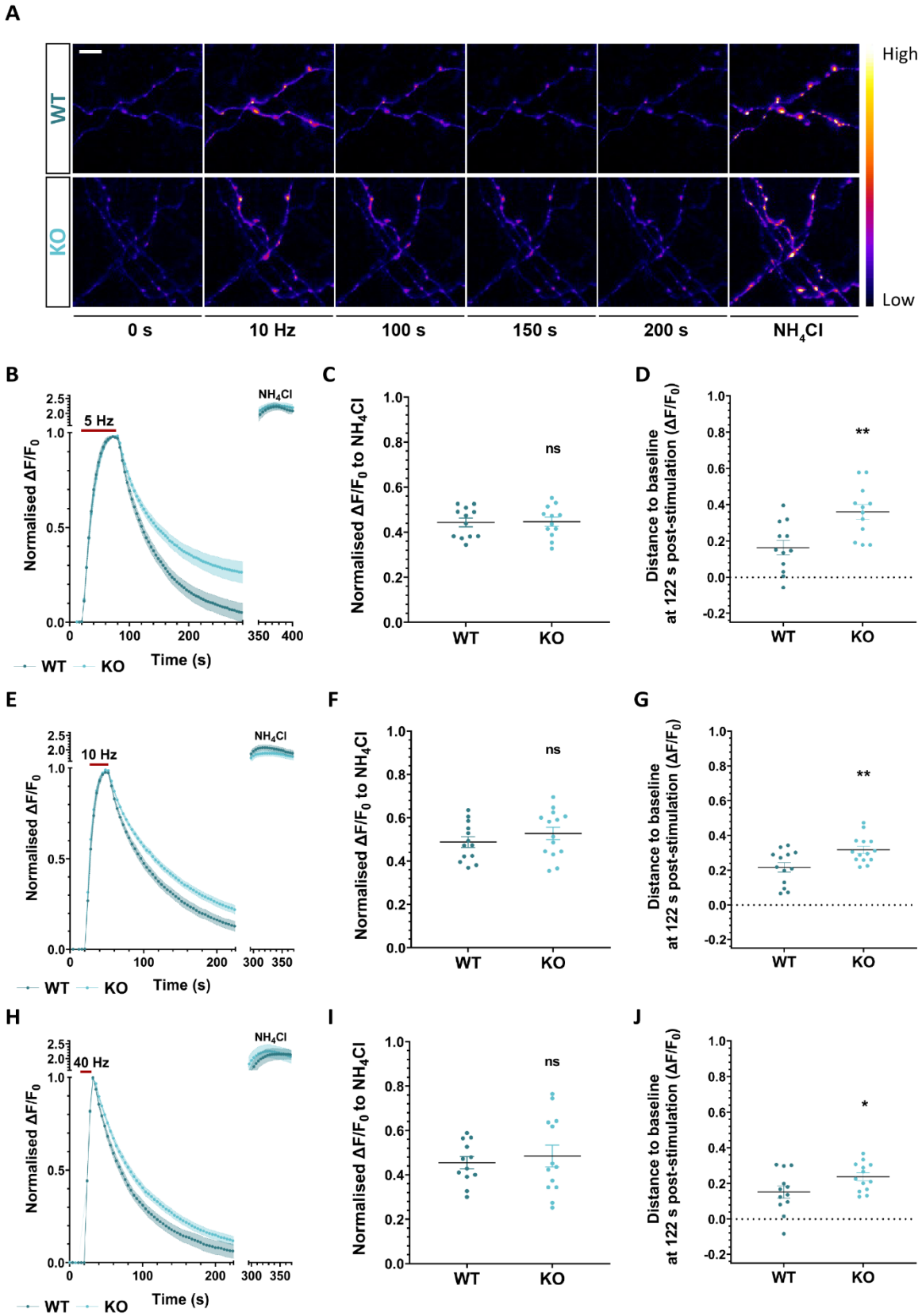

933 **Figure 3.** Loss of CDKL5 impairs the kinetics of SV endocytosis but not SV exocytosis. Primary
934 hippocampal neurons from WT and CDKL5 KO rats were transfected with sypHy at 8-9 DIV
935 and used at 13-14 DIV. (*A*) Example responses from sypHy-expressing axons that were
936 subjected to 300 APs at 10 Hz and perfused with NH_4Cl solution 3 min after termination of

937 stimulation. Representative image slices were selected from the time-course that was
938 recorded from both WT (top) and CDKL5 KO neuronal cultures (bottom). Scale bar, 5 µm.
939 SypHy response from neurons stimulated with either 300 APs at 5 Hz (*B*), 300 APs at 10 Hz (*E*),
940 or 400 APs at 40 Hz (*H*) (red bars) normalised to the stimulation peak ($\Delta F/F_0$). (*C*, *F*, *I*) SypHy
941 fluorescence ($\Delta F/F_0$) at stimulation peak when total sypHy response was normalised to NH_4Cl.
942 (*D*, *G*, *J*) sypHy fluorescence ($\Delta F/F_0$) measuring the distance from baseline at 122 s post-
943 stimulation. Scatter plots indicate mean ± SEM. ns, not significant, *$p < 0.05$, **$p < 0.01$ by
944 unpaired two-tailed *t* test. (*B*-*D*) WT $n = 12$, KO $n = 12$ coverslips from 4 independent
945 preparations of neuronal cultures. (*E*-*G*) WT $n = 13$, KO $n = 14$ coverslips from 4 independent
946 preparations of neuronal cultures. (*H*-*J*) WT $n = 12$, KO $n = 13$ coverslips from 4 independent
947 preparations of neuronal cultures.

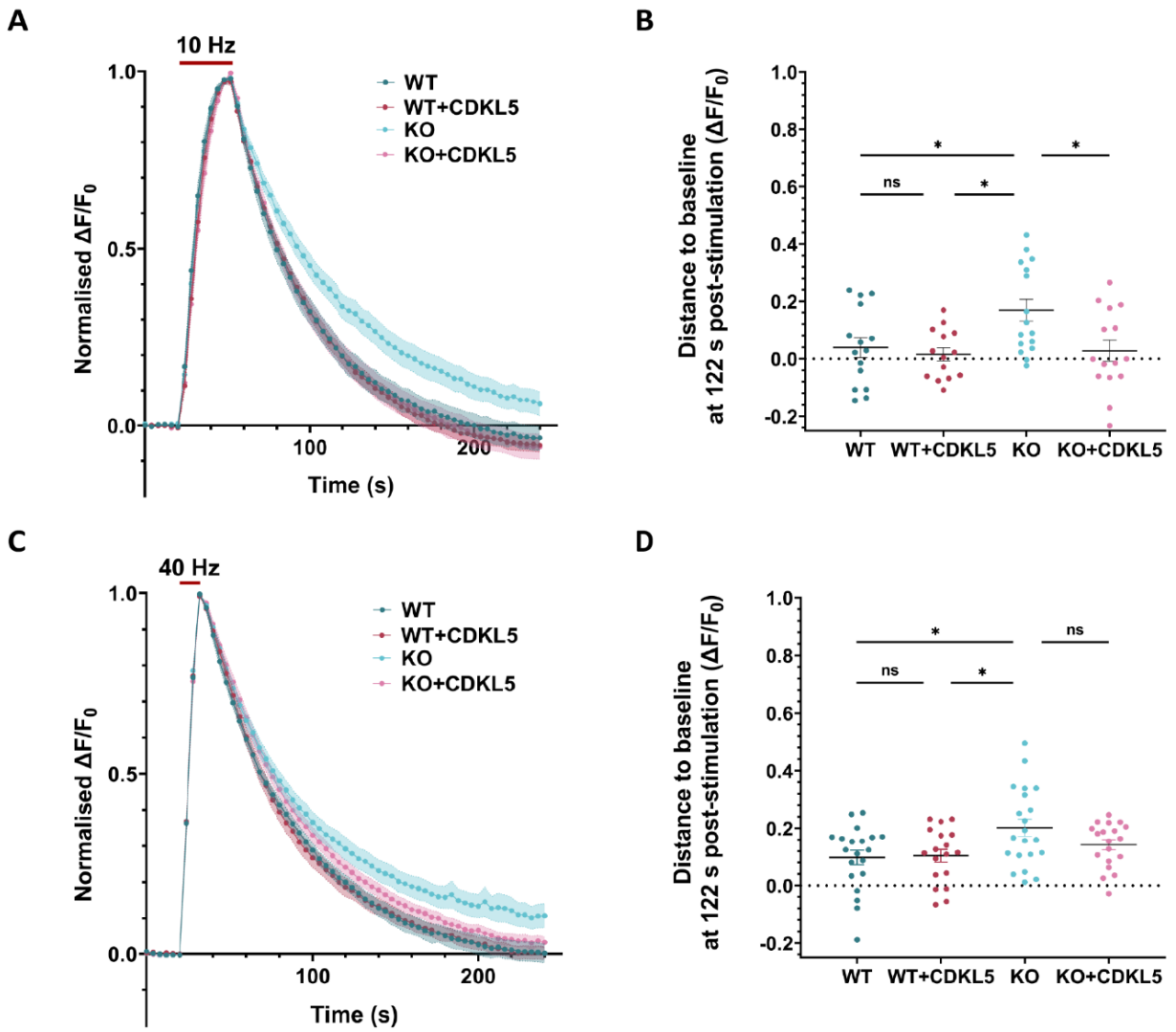

Figure 4. CDKL5 rescues the kinetics of SV endocytosis in CDKL5-deficient neurons. Primary hippocampal neurons from WT and CDKL5 KO rats were co-transfected with sypHy and mCer (WT, dark turquoise; KO, dark pink) or mCer-CDKL5 (WT+CDKL5, light turquoise; KO+CDKL5, light pink) at 8-9 DIV and used at 13-14 DIV. (*A*,*C*) sypHy response from neurons stimulated (red bar) with either 300 APs at 10 Hz (*A*) or 400 APs at 40 Hz (*C*) normalised to the stimulation peak and (*B*,*D*) sypHy fluorescence measuring the distance from baseline at 122 s post-stimulation. (*B*) Scatter plots indicate mean ± SEM. ns, not significant, *$p < 0.05$ by two-way ANOVA followed by Tukey's multiple comparison test. WT $n = 15$, WT+CDKL5 $n = 14$, KO $n = 16$, KO+CDKL5 $n = 15$ coverslips from 4 independent preparations of neuronal cultures. (*D*) Scatter plots indicate mean ± SEM. ns, not significant, *$p < 0.05$ by two-way ANOVA followed by Tukey's multiple comparison test. WT $n = 20$, WT+CDKL5 $n = 18$, KO $n = 21$, KO+CDKL5 $n = 19$ coverslips from 5 independent preparations of neuronal cultures.

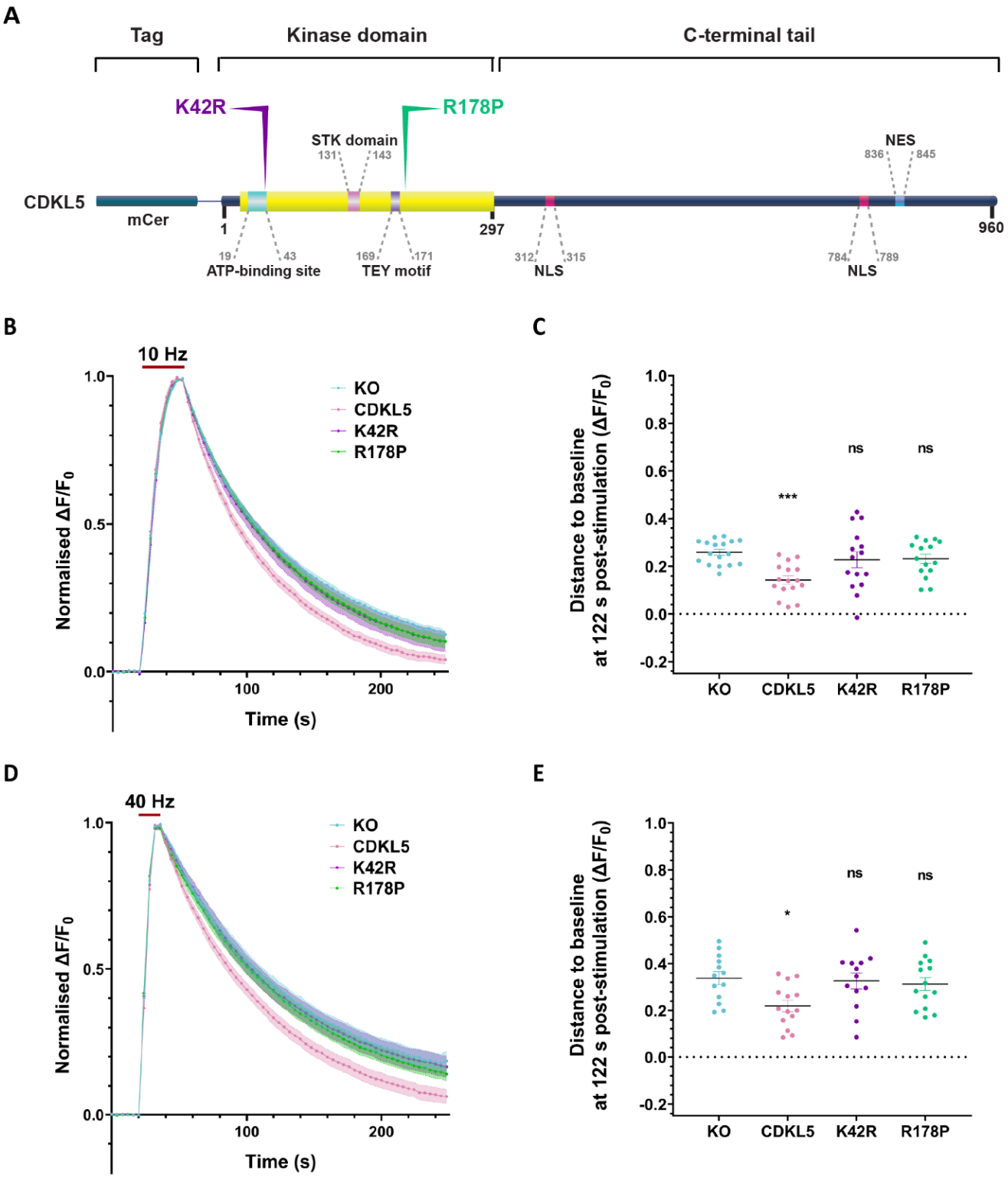

Figure 5. Point mutations within the CDKL5 kinase domain cannot correct SV endocytosis kinetics in CDKL5 KO neurons. (*A*) Schematic representation of the structural domains of CDKL5. Point mutations were introduced into the kinase domain including K42R, within the ATP-binding region, and R178P adjacent to the TEY motif. All constructs were tagged with mCer at their N-termini. (*B-E*) Primary hippocampal neurons from CDKL5 KO rats were co-transfected with sypHy and mCer (KO, light turquoise), mCer-CDKL5 (CDKL5, light pink), K42R (purple) or R178P (green) at 8-9 DIV and used at 13-14 DIV. (*B*,*D*) sypHy response from

967 neurons stimulated (red bar) with either 300 APs at 10 Hz (*B*) or 400 APs at 40 Hz (*D*)
968 normalised to the stimulation peak. (*C*,*E*) SypHy fluorescence measuring the distance from
969 baseline at 122 s post-stimulation. (*C*) Scatter plots indicate mean ± SEM. ns, not significant,
970 ***$p < 0.001$ by one-way ANOVA followed by Dunnett's multiple comparison test. KO $n = 17$,
971 CDKL5 $n = 16$, K42R $n = 15$, R178P $n = 15$ coverslips from 5 independent preparations of
972 neuronal cultures. (*E*) Scatter plots indicate mean ± SEM. ns, not significant, *$p < 0.05$ by one-
973 way ANOVA followed by Dunnett's multiple comparison test. KO $n = 13$, CDKL5 $n = 14$, K42R
974 $n = 13$, R178P $n = 14$ coverslips from 4 independent preparations of neuronal cultures.

975

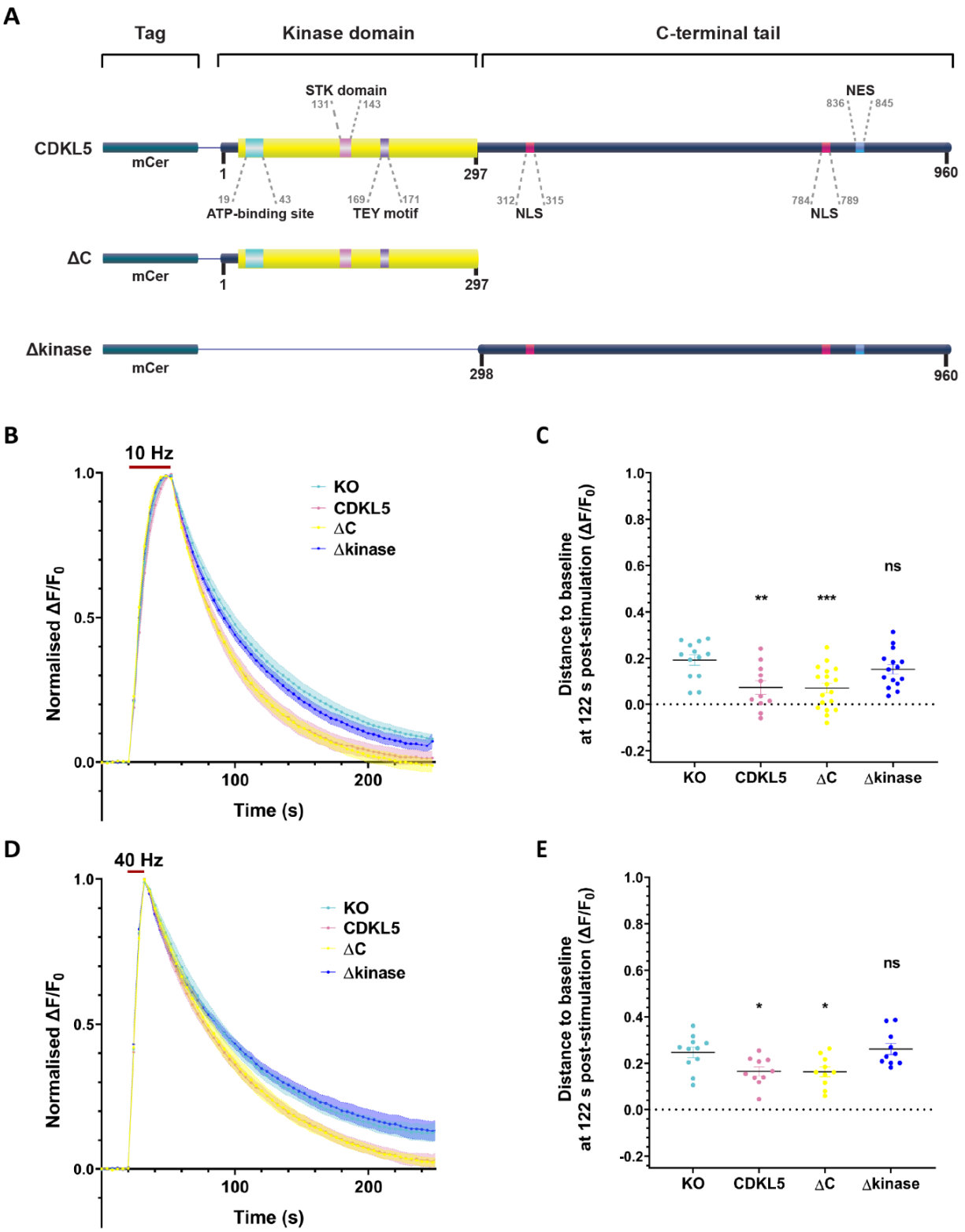

Figure 6. The CDKL5 kinase domain is sufficient to restore the SV endocytosis kinetics in CDKL5 KO neurons. (*A*) Schematic representation of the structural domains of CDKL5. Truncated versions of CDKL5 were generated comprising either the kinase domain (ΔC) or the C-terminal tail (Δkinase). All constructs were tagged with mCer at their N-termini. (*B-E*) Primary hippocampal neurons from CDKL5 KO rats were co-transfected with sypHy and mCer (KO, light turquoise), mCer-CDKL5 (CDKL5, light pink), the kinase domain (ΔC, yellow) or the C-

982 terminal tail (Δkinase, blue) at 8-9 DIV and used at 13-14 DIV. (*B*,*D*) sypHy response from
983 neurons challenged (red bar) with either 300 APs at 10 Hz (*B*) or 400 APs at 40 Hz (*D*)
984 normalised to the stimulation peak. (*C,E*) sypHy fluorescence measuring the distance from
985 baseline at 122 s post-stimulation. (*C*) Scatter plots indicate mean ± SEM. ns, not significant,
986 $**p < 0.01$, $***p < 0.001$ by one-way ANOVA followed by Dunnett's multiple comparison test.
987 KO $n = 13$, CDKL5 $n = 11$, ΔC $n = 18$, Δkinase $n = 15$ coverslips from 4 independent preparations
988 of neuronal cultures. (*E*) Scatter plots indicate mean ± SEM. ns, not significant $*p < 0.05$ by
989 one-way ANOVA followed by Dunnett's multiple comparison test. KO $n = 11$, CDKL5 $n = 10$, ΔC
990 $n = 10$, Δkinase $n = 10$ coverslips from 3 independent preparations of neuronal cultures.

991

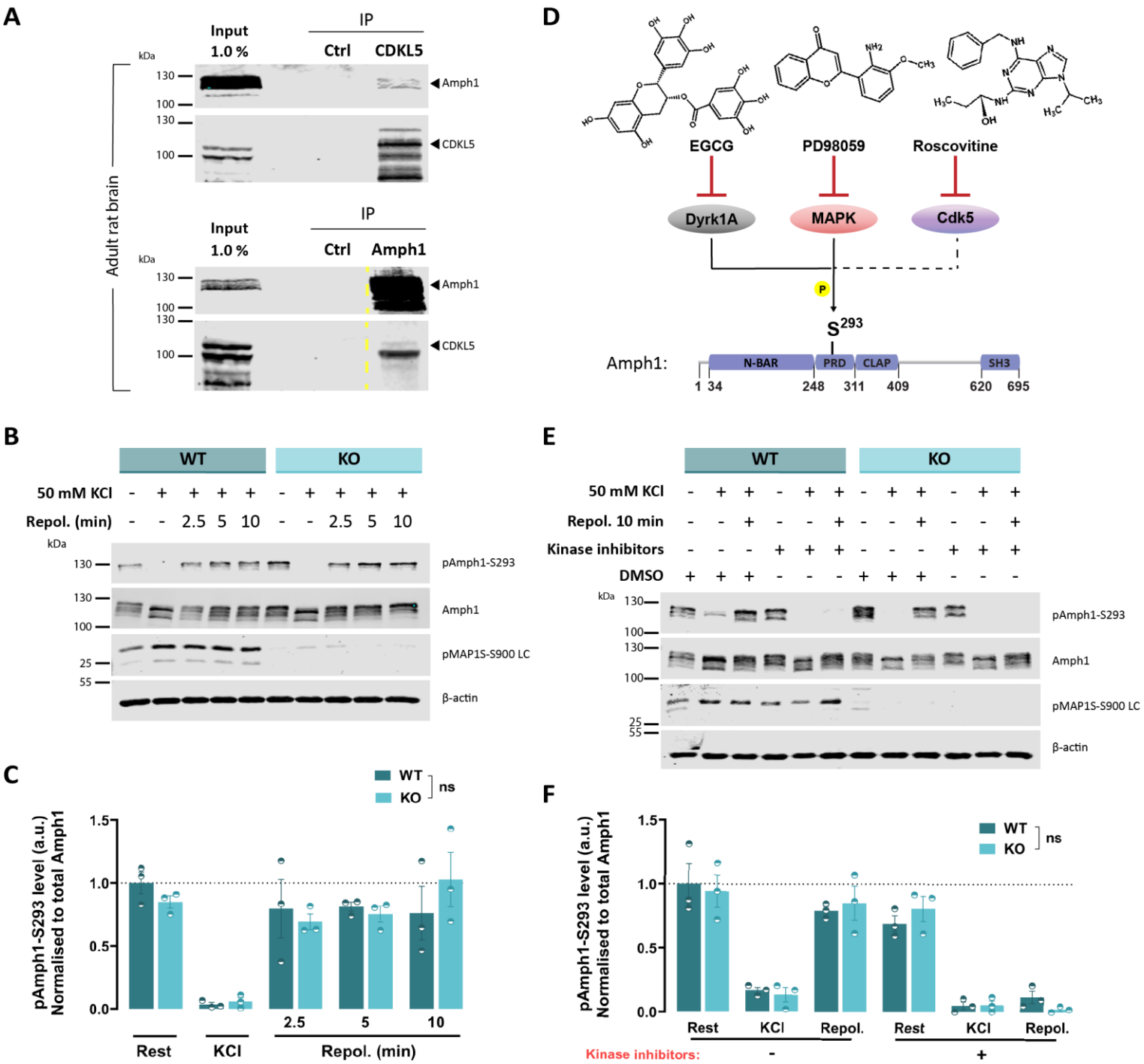

Figure 7. Amph1-S293 is phosphorylated independently of CDKL5. (*A*) Co-immunoprecipitation from adult rat brain lysates of Amph1 and CDKL5 with CDKL5 and Amph1 antibodies, respectively. Dashed lines indicate cropped images. (*B*) Primary hippocampal neurons at 14-15 DIV from WT and CDKL5 KO rats were depolarised with 50 mM KCl for 2 min and allowed to repolarise for 2.5, 5, and 10 min, respectively. Neurons were analysed for pAmph1-S293, Amph1, pMAP1S-S900 LC, and β-actin. (*C*) Quantification of the phosphorylation levels of Amph1-S293 normalised to total Amph1. Bars indicate mean ± SEM. ns, not significant by two-way ANOVA followed by Sidak's multiple comparison test. WT n = 3 coverslips/condition, KO n = 3 coverslips/condition from 3 independent preparations of

1001 neuronal cultures. (*D*) EGCG, PD98059, and roscovitine were combined to block the kinase
1002 activity of Dyrk1A, MAPK, and Cdk5, respectively. All three kinases phosphorylate Amph1 in
1003 neurons with Dyrk1A and MAPK (continuous lines) and possibly Cdk5 (dashed line) also
1004 targeting S293. The skeletal structures of the inhibitors were generated by ACD/ChemSketch,
1005 2021.1.0. (*E*) Hippocampal neurons at 14-15 DIV derived from WT and CDKL5 KO rats were
1006 treated with 20 mM EGCG, 100 µM PD98059, and 50 µM roscovitine inhibitors combined
1007 together for 1 h and stimulated with 50 mM KCl prior to repolarisation for 10 min in the
1008 presence of kinase inhibitors, or appropriate amount of DMSO. Lysates were assessed for
1009 pAmph1-S293, Amph1, pMAP1S-S900 LC, and β-actin. (*F*) Quantification of pAmph1-S293
1010 levels normalised to total Amph1. Background was subtracted in all cases. Bars indicate mean
1011 ± SEM. ns, not significant by two-way ANOVA followed by Sidak's multiple comparison test.
1012 WT n = 3 coverslips/condition, KO n = 3 coverslips/condition from 3 independent preparations
1013 of neuronal cultures.